

Supporting Information

Assembled bis-urea macrocycles: Exploring photodriven electron transfer from host to guests.

Md Faizul Islam, Ammon J. Sindt, Muhammad Saddam Hossain, Pooja J. Ayare, Mark D. Smith, Aaron K. Vannucci, Sophya Garashchuk and Linda S. Shimizu*

Department of Chemistry and Biochemistry, University of South Carolina, Columbia, South Carolina 29208, United States.

Fax: 803-777-9521; Tel: 803-777-2066

Email: SHIMIZLS@mailbox.sc.edu

Contents

General experimental	2
Characterization of compounds	3
UV irradiation of the samples and light flux for 365 nm LEDs	8
Interaction between macrocycle units	9
Crystal data and structure refinement	10
Iodine loading in cyclohexane	21
Iodine removal in ethanol	22
Solid state Raman spectrum	24
X-ray Photoelectron measurements	26
Infrared Measurements	27
Absorbance Measurements	28
Photoluminescence Measurements	29
Cyclic Voltammetry	31
Tauc Plot	36
Electron Paramagnetic Resonance (EPR) Measurements	37
NMR spectra pre and post UV	39
IR spectra pre and post UV	41
Computational Details	42

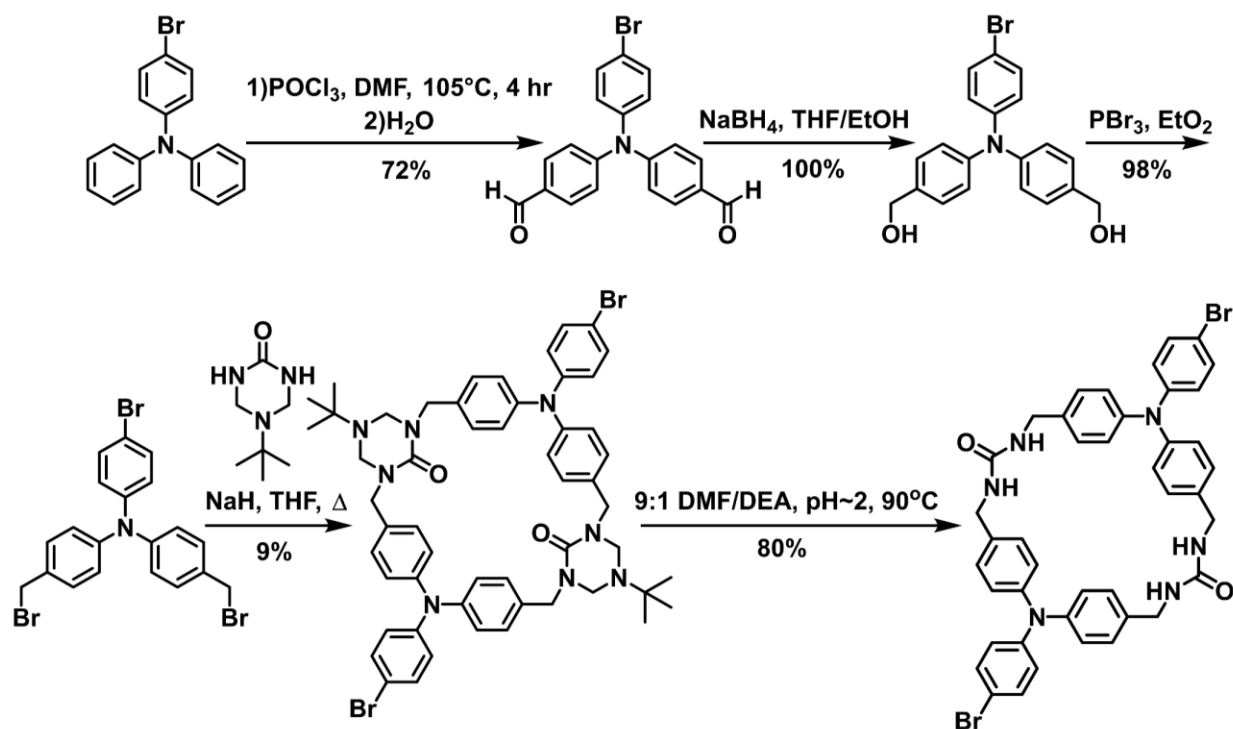
General Experimental

NMR spectra were recorded on Bruker Advance 300 MHz spectrometers. Chemical shifts are reported in ppm (δ) and were internally referenced with the solvent peak. All chemicals were purchased from chemical suppliers and were used as received unless otherwise noted. UV-irradiation of all materials were carried out with 365 nm LEDs. Samples were purged with argon before irradiation. All other instrument protocols are described in their own sections.

Synthesis of Host 1.

Host 1 was synthesized according to the previous procedure.¹

Scheme S1: Synthesis of Host 1



Characterization of compounds

^1H NMR $1 \bullet \text{DME}$

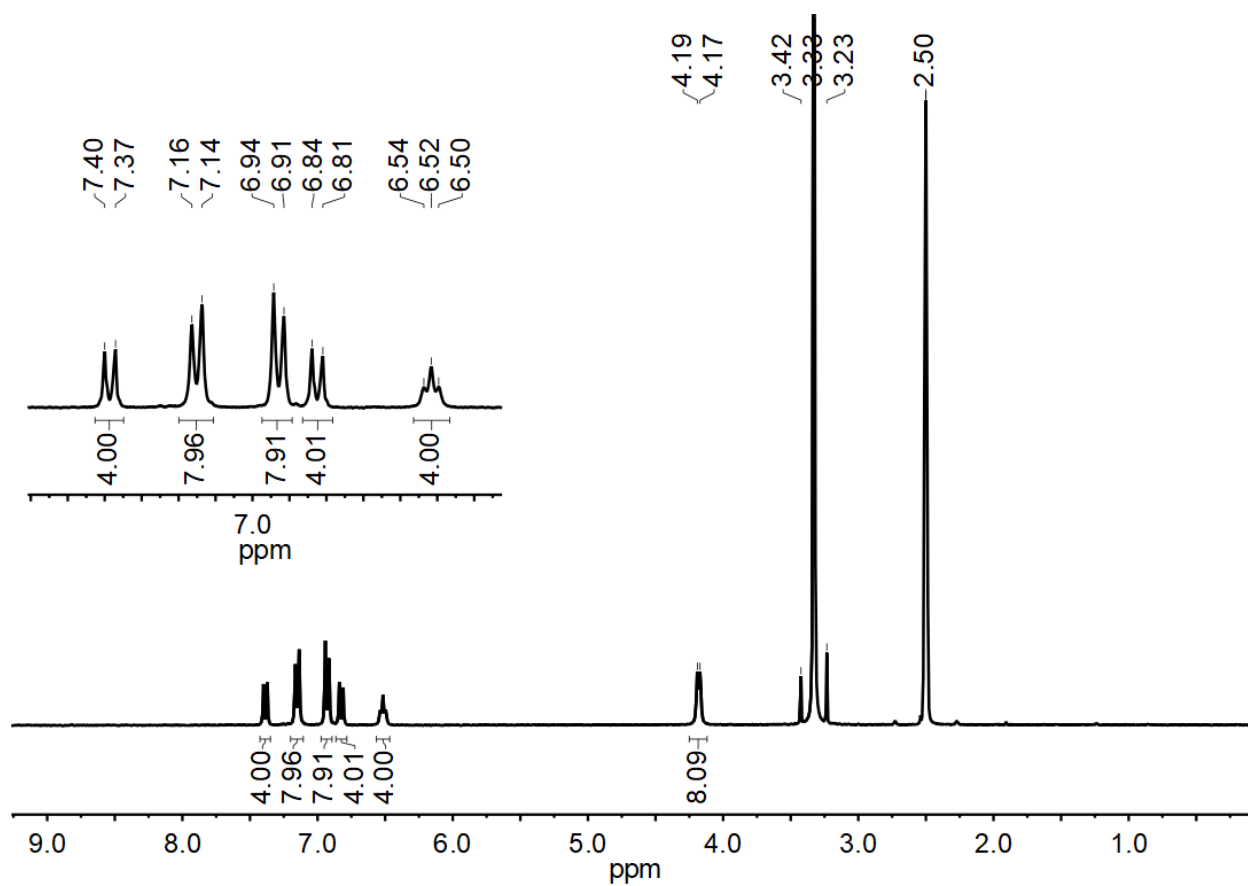


Figure S1. ^1H NMR of $1 \bullet \text{DME}$ (300 MHz, DMSO) δ 7.39 (d, $J = 8.8$ Hz, 4H), 7.15 (d, $J = 8.3$ Hz, 8H), 6.93 (d, $J = 8.3$ Hz, 8H), 6.82 (d, $J = 8.8$ Hz, 4H), 6.52 (t, $J = 6.0$ Hz, 4H), 4.18 (d, $J = 5.9$ Hz, 8H).

^1H NMR of $1 \cdot \text{C}_6\text{H}_4\text{N}_2\text{S}$

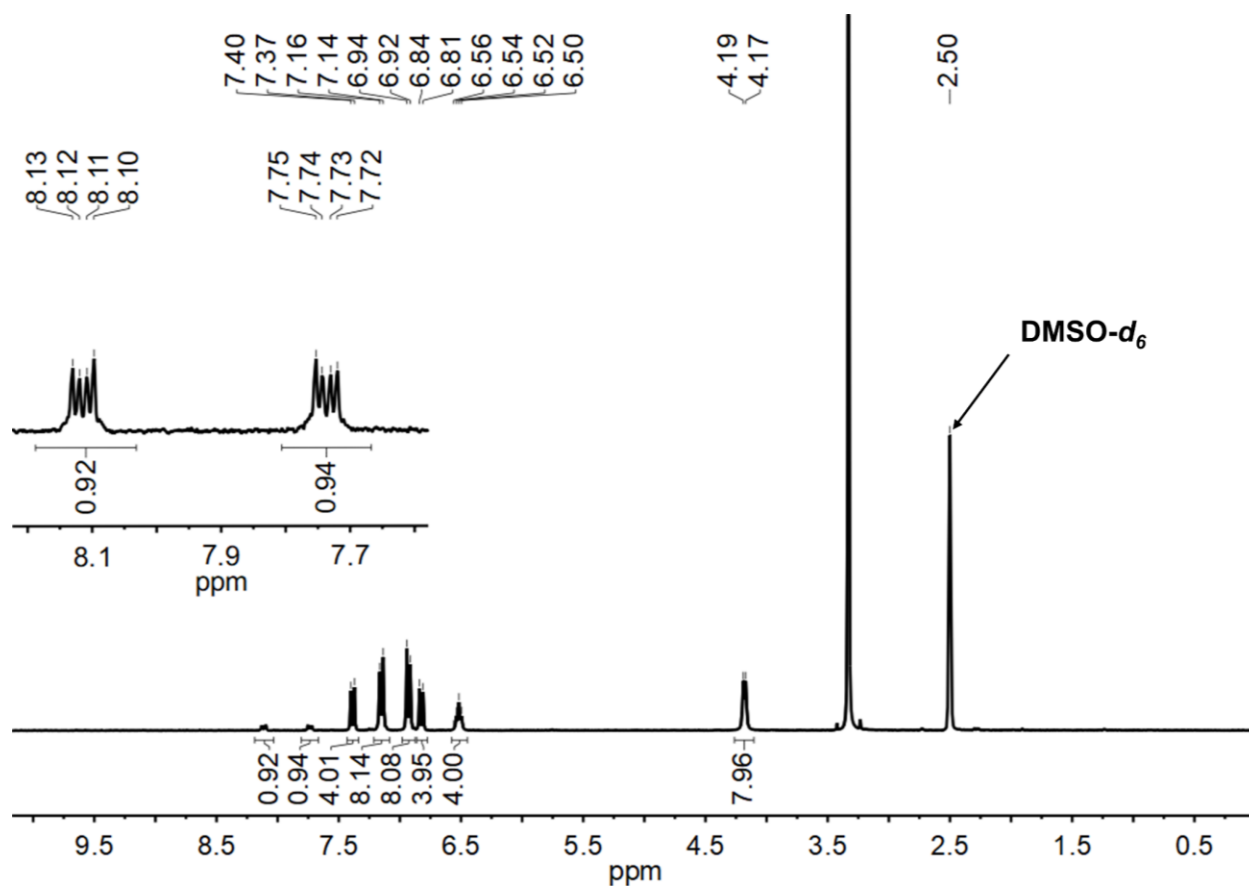


Figure S2. ^1H NMR of $1 \cdot \text{C}_6\text{H}_4\text{N}_2\text{S}$ (300 MHz, DMSO) δ 8.11 (dd, $J = 6.7, 3.2$ Hz, 1H), 7.74 (dd, $J = 7.0, 3.0$ Hz, 1H), 7.39 (d, $J = 8.8$ Hz, 4H), 7.15 (d, $J = 8.3$ Hz, 8H), 6.93 (d, $J = 8.3$ Hz, 8H), 6.82 (d, $J = 8.8$ Hz, 4H), 6.52 (t, $J = 6.2$ Hz, 4H), 4.18 (d, $J = 5.9$ Hz, 8H).

^1H NMR of $1 \cdot \text{C}_6\text{H}_2\text{Cl}_2\text{O}_2$

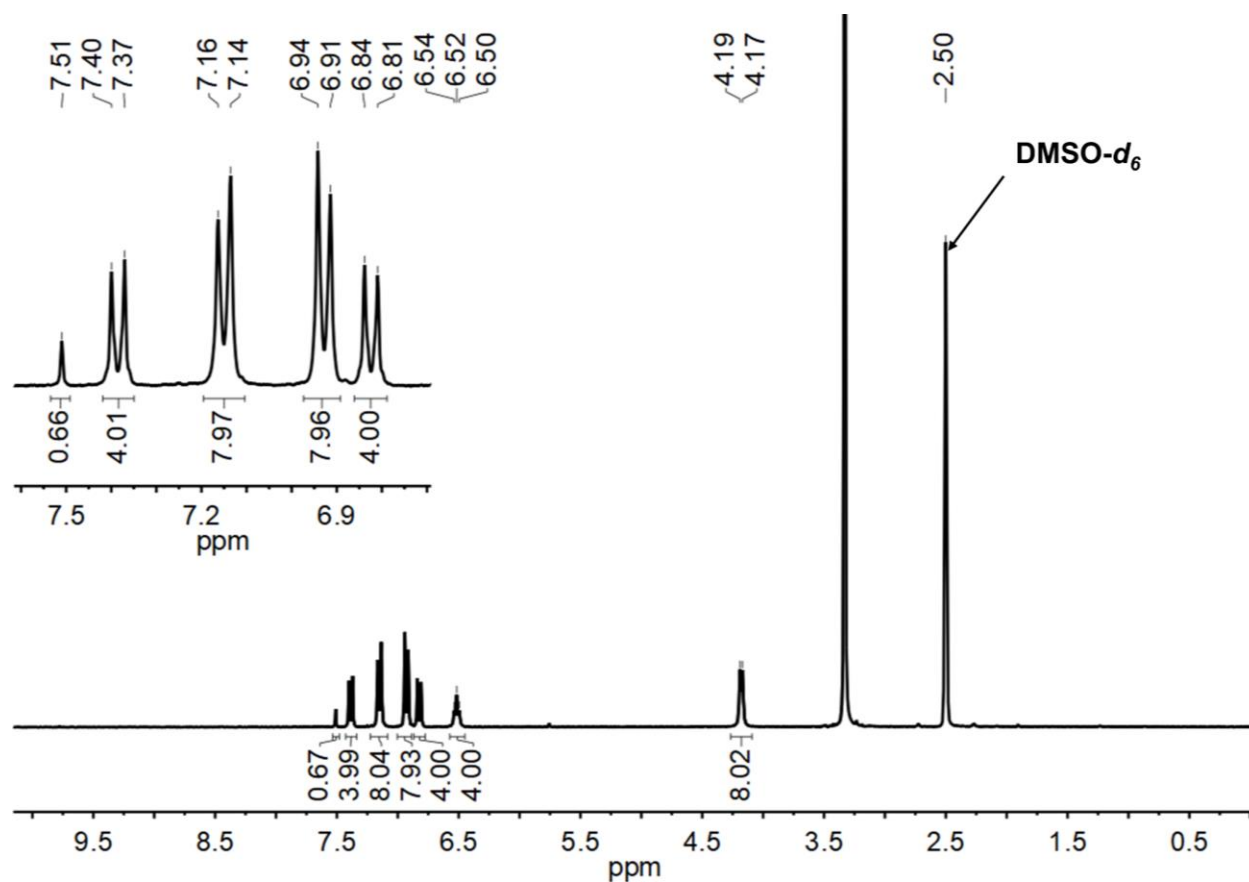


Figure S3. ^1H NMR of $1 \cdot \text{C}_6\text{H}_2\text{Cl}_2\text{O}_2$ (300 MHz, DMSO) δ 7.51 (s, 1H), 7.38 (d, $J = 8.8$ Hz, 4H), 7.15 (d, $J = 8.3$ Hz, 8H), 6.93 (d, $J = 8.3$ Hz, 8H), 6.82 (d, $J = 8.8$ Hz, 4H), 6.52 (t, $J = 6.2$ Hz, 4H), 4.18 (d, $J = 6.0$ Hz, 8H).

^1H NMR of $1 \bullet \text{I}_2$

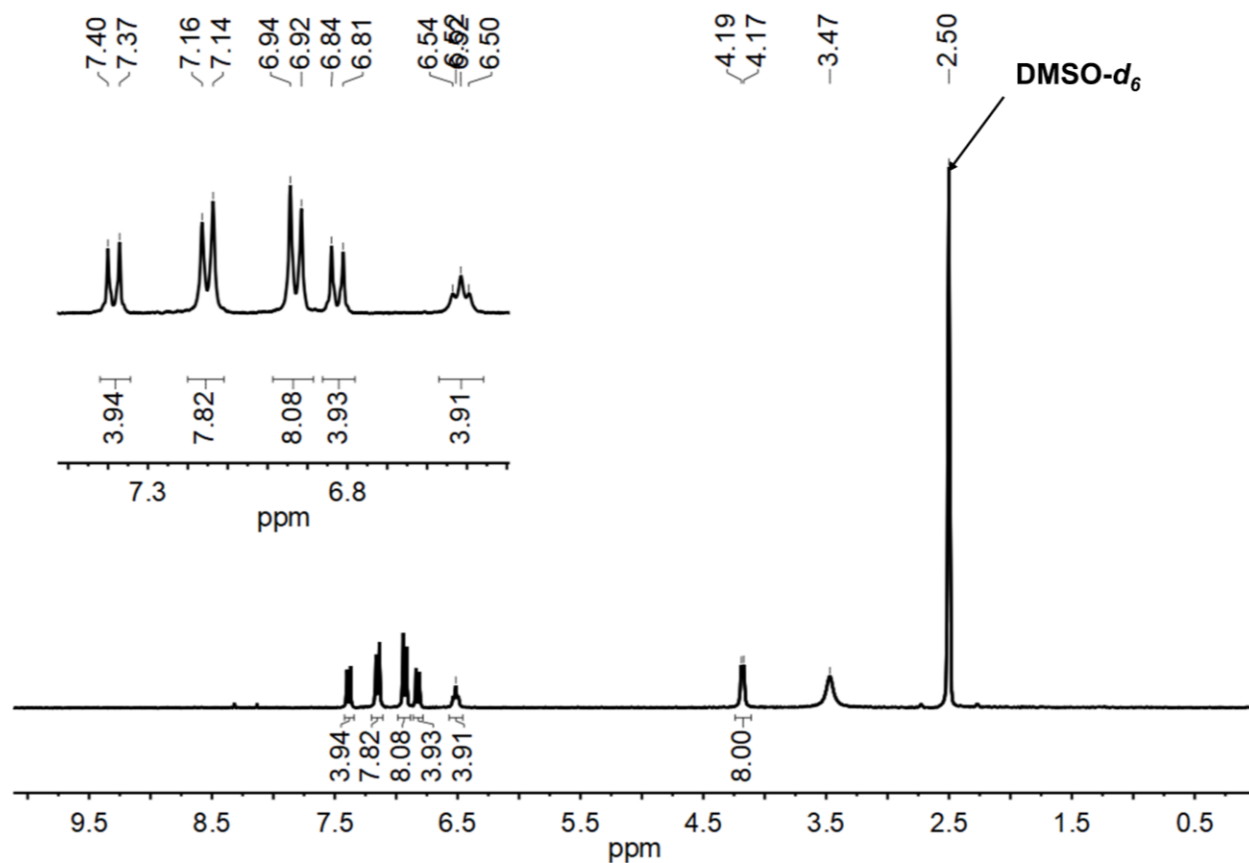


Figure S4. ^1H NMR of $1 \bullet \text{I}_2$ (300 MHz, DMSO) δ 7.39 (d, $J = 8.7$ Hz, 4H), 7.15 (d, $J = 8.3$ Hz, 8H), 6.93 (d, $J = 8.4$ Hz, 8H), 6.82 (d, $J = 8.7$ Hz, 4H), 6.52 (t, $J = 6.1$ Hz, 4H), 4.18 (d, $J = 5.7$ Hz, 8H).

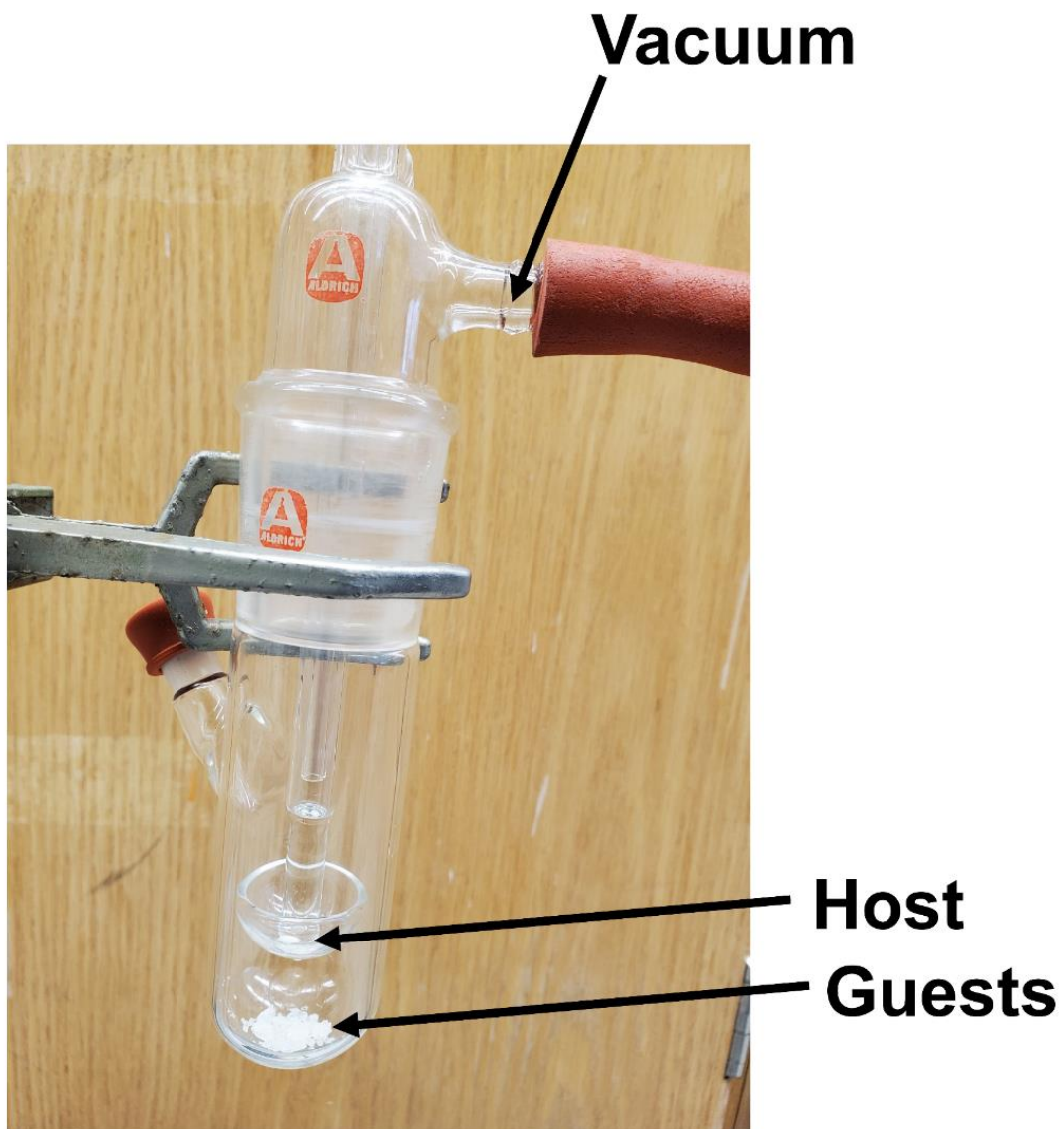


Figure S5. Guest loading apparatus

UV irradiation of the samples and light flux for 365 nm LEDs

Samples were dried under Ar(g) and loaded in EPR tubes, which were oriented horizontally and exposed to 365 nm Waveform lighting real UV LED strips (4.5 W/ft, 3.2 ft). The photon flux was estimated as 9.78×10^{15} photons/sec.

Sample	Measured Current (amps)
Background	4.1×10^{-11}
LED 1	2.13×10^{-6}
LED 2	2.29×10^{-6}
LED 3	2.25×10^{-6}
LED 4	2.04×10^{-6}
LED 5	2.40×10^{-6}
Average	2.22×10^{-6}
Background subtracted average	2.22×10^{-6}
Multiplied by number of LEDs in photoreactor (120)	2.67×10^{-4}

To measure the photon flux of the 365 nm LED photoreactor FDS100 photodiode from ThorLabs were used. As the sample distance in the photoreactor is around 3.5 cm, individual LED currents were measured at the same distance too. Average current was measured for 5 LEDs and ambient light background was subtracted and then multiplied by the number of LEDs in the photoreactor(120). Power of LEDs was calculated by dividing the current value by the responsivity of the photodiode (0.05 amps/watts at 365 nm) at the sample distance (5.33×10^{-3} watts).

Solving for E in the equation for photon energy ($E = \frac{hc}{\lambda}$) with $\lambda = 365$ nm, gives a photon energy value of 5.45×10^{-19} J. Division of the measured wattage by the photon energy gives a photon flux value of 9.78×10^{15} photons/second delivered to the sample for all measurements.

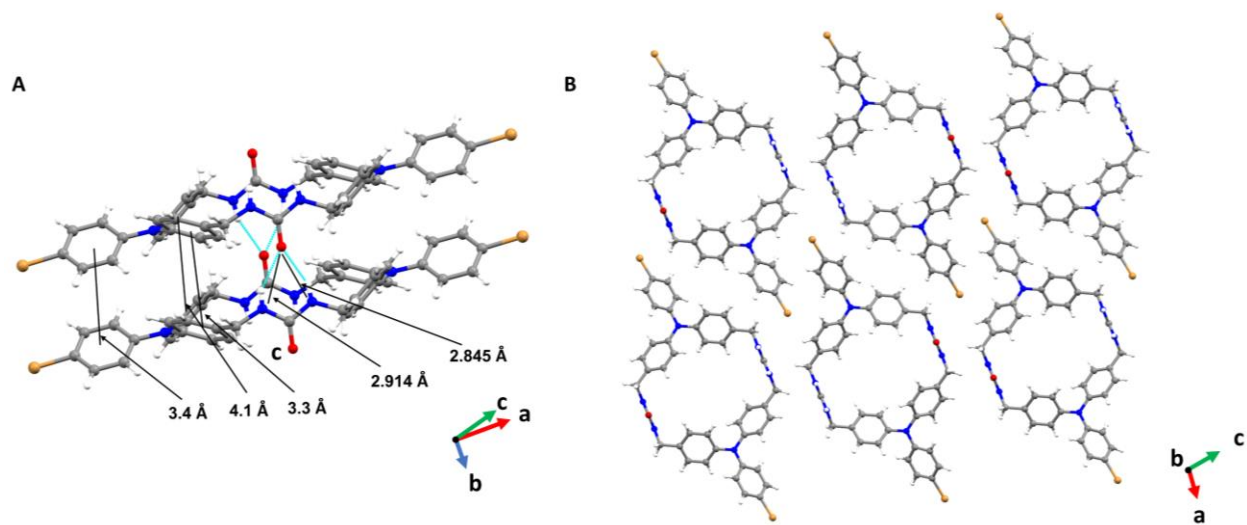


Figure S6. A) π -stacking in-between the macrocycles. The three phenyl rings of the TPA unit are aligned in an offset π -stacking arrangement with perpendicular distances of 3.304(14), 3.368(14), and 4.125(15) Å. B) Packing of the macrocycles towards c-axis.

Crystal data and structure refinement

Structure $1 \cdot C_6H_4N_2S$

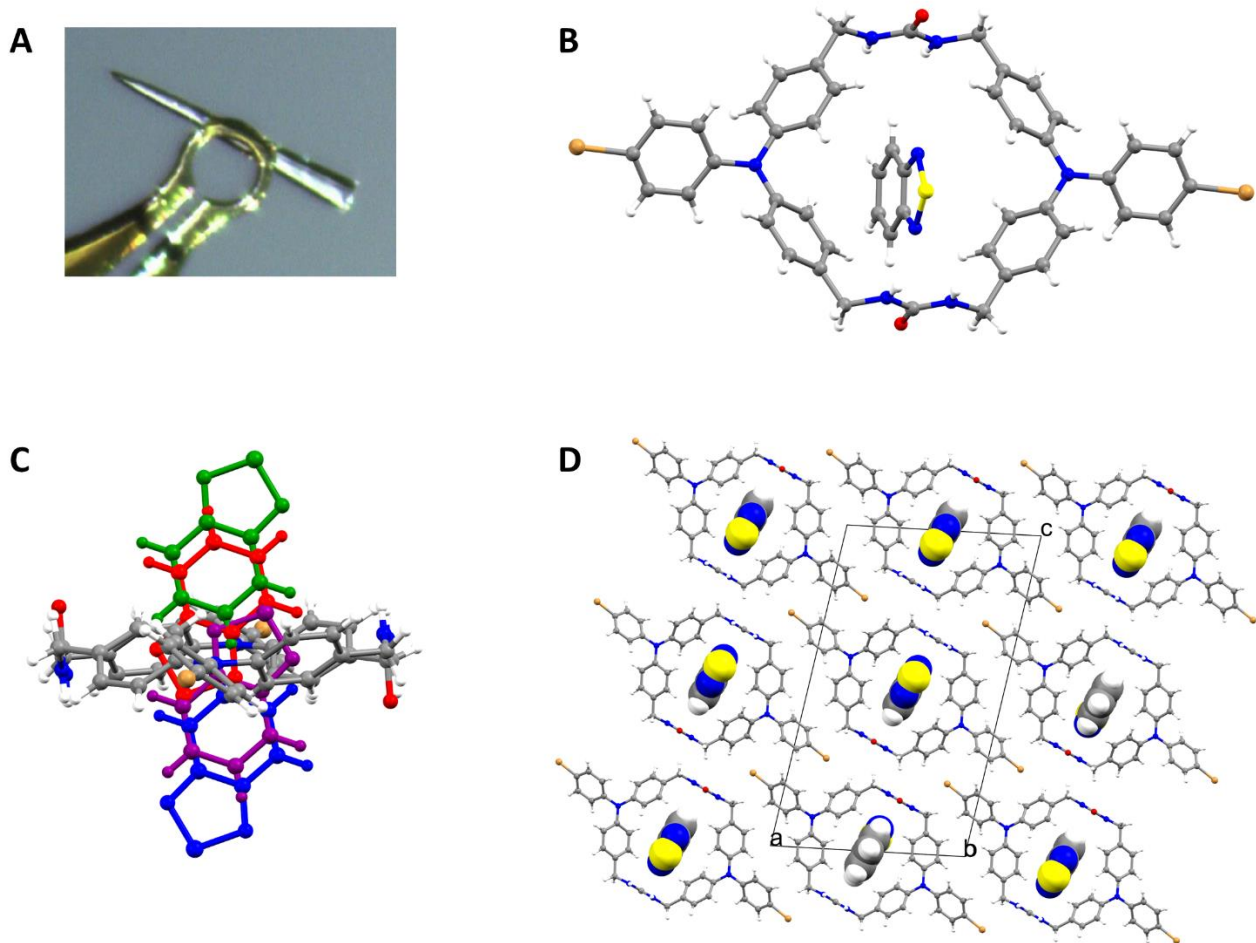


Figure S7. Crystal views of $1 \cdot C_6H_4N_2S$. A) Data crystal, B) Components of structure, C) View of $C_6H_4N_2S$ disorder inside the host **1**, D) Crystal packing along a -axis.

X-ray intensity data from colorless needle were collected at 100(2) K using a Bruker D8 QUEST diffractometer equipped with a PHOTON-100 CMOS area detector and an Incoatec microfocus source (Mo $K\alpha$ radiation, $\lambda = 0.71073 \text{ \AA}$). The raw area detector data frames were reduced and corrected for absorption effects using the Bruker APEX3, SAINT+ and SADABS programs.^{1,2} The structure was solved with SHELXT.³ Subsequent difference Fourier calculations and full-matrix least-squares refinement against F^2 were performed with SHELXL-2018³ using OLEX2.⁴

The compound crystallizes in the monoclinic system. The pattern of systematic absences in the intensity data was consistent with the space group $P2_1/c$, which was confirmed by structure solution. The asymmetric unit consists of half of one $C_{42}H_{36}Br_2N_6O_2$ cycle located on a crystallographic inversion center and several electron density peaks inside the tubular channels created by the cycle columns. The residual electron density in the channel region is disordered, but generally arranged in a planar, tapelike fashion along the crystallographic b axis direction. If assigned as carbon atoms, most peaks refined to much less than full occupancy. One peak was significantly greater in magnitude and was assigned as the sulfur atom from the benzothiadiazole guest. Other difference map peaks could be fitted to the nitrogen and carbon atoms of the guest. The benzothiadiazole is disordered over two symmetry-equivalent sites per unit cell. Preliminary disorder refinements gave a molecular occupancy near 0.25. For steric reasons, the final occupancy value was fixed at 0.25, giving a composition per cycle of 0.5. 1,2- S-N and C-N and 1,3- S-C and N-C distances in the benzothiadiazole guest were restrained to reasonable values taken from the literature. The phenyl ring was fitted to a rigid hexagon with $d(C-C) = 1.39 \text{ \AA}$. Only the sulfur atom of the guest was refined anisotropically; phenyl carbon and the nitrogen atoms were given a common isotropic displacement parameter. All non-hydrogen atoms of the cycle were refined with anisotropic displacement parameters. Hydrogen atoms bonded to carbon were placed in geometrically idealized positions and included as riding atoms with $d(C-H) = 0.95 \text{ \AA}$ and $U_{iso}(H) = 1.2U_{eq}(C)$ for arene hydrogen atoms and $d(C-H) = 0.99 \text{ \AA}$ and $U_{iso}(H) = 1.2U_{eq}(C)$ for methylene hydrogen atoms. The two urea hydrogen atoms were located in difference maps and refined isotropically with $d(N-H) = 0.85(2)$ distance restraints and a common isotropic displacement parameter. The largest residual electron density peak in the final difference map is $0.50 \text{ e}^-/\text{\AA}^3$, located 0.70 \AA from C4S.

Structure 1 • C₆H₂Cl₂O₂

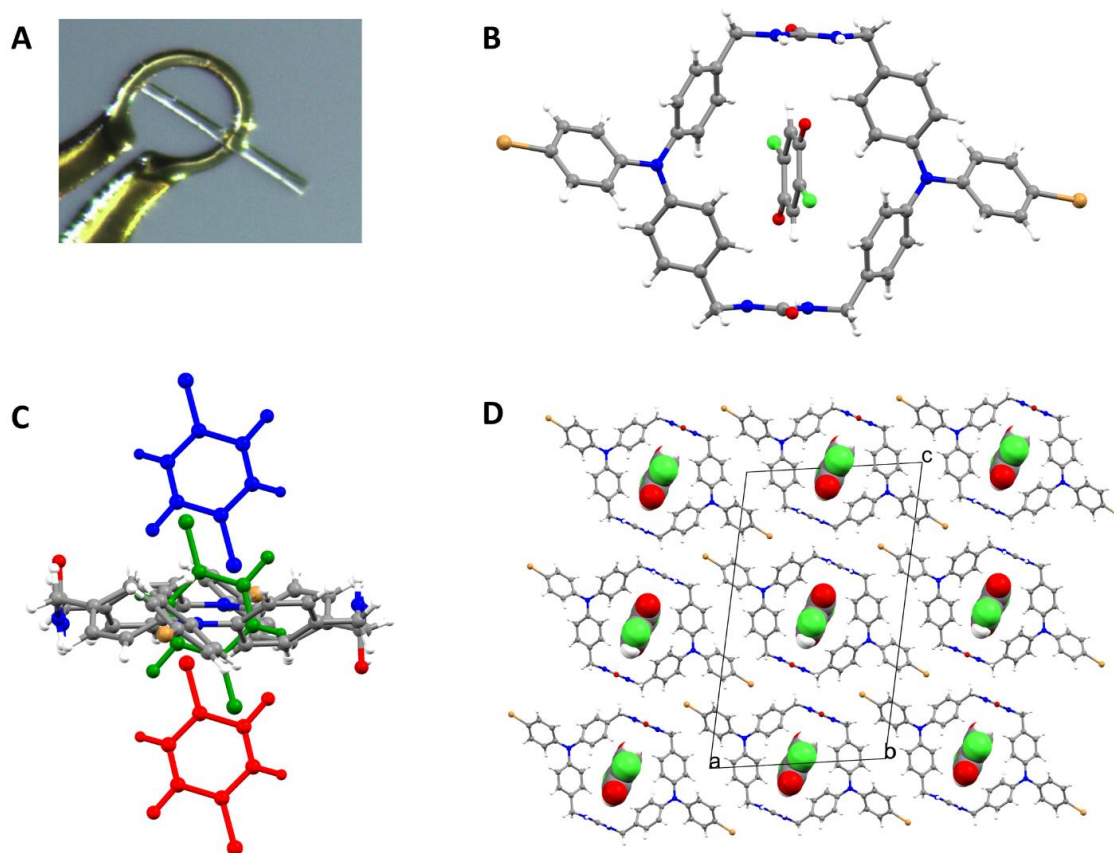


Figure S8. Crystal views of **1**•C₆H₂Cl₂O₂. A) Data crystal, B) Components of structure, C) arrangement of three symmetry equivalent C₆H₂Cl₂O₂ guests relative to one cycle of host **1**, D) Crystal packing along *a*-axis.

X-ray intensity data from a colorless needle were collected at 100(2) K using a Bruker D8 QUEST diffractometer equipped with a PHOTON-100 CMOS area detector and an Incoatec microfocus source (Mo K α radiation, $\lambda = 0.71073$ Å). The raw area detector data frames were reduced, scaled and corrected for absorption effects using the Bruker APEX3, SAINT+ and SADABS programs.^{1,2} The structure was solved with SHELXT.³ Subsequent difference Fourier calculations and full-matrix least-squares refinement against F^2 were performed with SHELXL-2018³ using OLEX2.⁴

The compound crystallizes in the monoclinic system. The pattern of systematic absences in the intensity data was uniquely consistent with the space group $P2_1/c$, which was confirmed by structure solution. The ordered part of the asymmetric unit consists of half of one

$C_{42}H_{36}Br_2N_6O_2$ cycle located on a crystallographic inversion center. Five additional electron density peaks were observed located inside tubular channels created by columns of $C_{42}H_{36}Br_2N_6O_2$ molecules. The residual electron density in the channel region is arranged in a planar, tapelike fashion along the crystallographic b axis direction. The five peaks modeled well as half (three carbon, one oxygen and one chlorine atom) of a partially occupied 2,5-dichloro-1,4-benzoquinone ($C_6H_2Cl_2O_2$) molecule, also located on a crystallographic inversion center. Refinement of the Cl_2BQ group occupancy parameter gave 0.31(1). C-Cl, C-O, and C-C distance restraints were applied to the Cl_2BQ guest to maintain a chemically reasonable geometry. Expected $C_6H_2Cl_2O_2$ distances were taken from the literature. All non-hydrogen atoms were refined with anisotropic displacement parameters except for atoms of the disordered $C_6H_2Cl_2O_2$ guest, which were refined isotropically. Hydrogen atoms bonded to carbon were located in Fourier difference maps before being placed in geometrically idealized positions and included as riding atoms with $d(C-H) = 0.95 \text{ \AA}$ and $U_{iso}(H) = 1.2U_{eq}(C)$ for arene hydrogen atoms and $d(C-H) = 0.99 \text{ \AA}$ and $U_{iso}(H) = 1.2U_{eq}(C)$ for methylene hydrogen atoms. The two urea hydrogen atoms were located in difference maps and refined isotropically with $d(N-H) = 0.85(2)$ distance restraints. The largest residual electron density peak in the final difference map is $0.79 \text{ e}^-/\text{\AA}^3$, located 1.23 \AA from Br1.

Structure 1•I₂

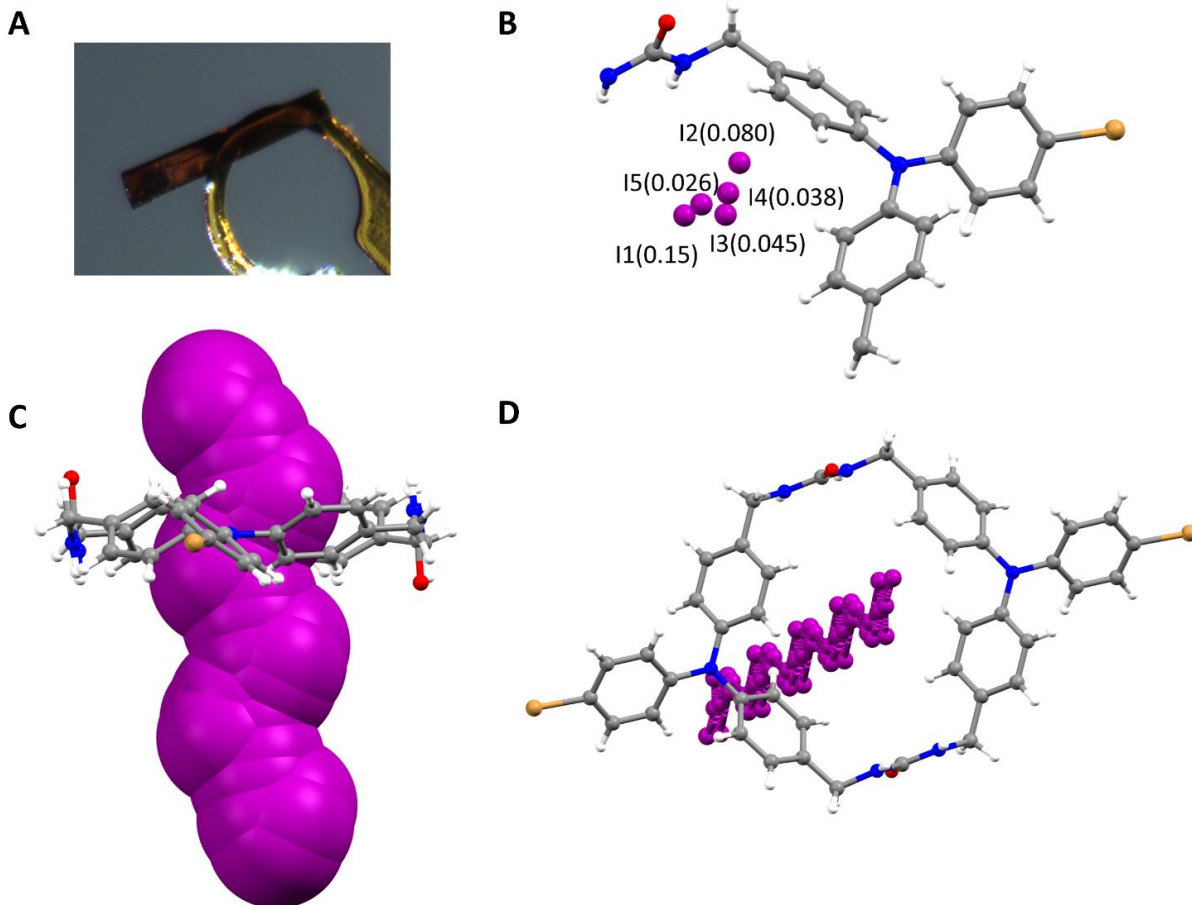


Figure S9. Crystal views of **1**•C₆H₂Cl₂O₂. A) Data crystal, B) Asymmetric unit of the crystal. Cycle interior contains disordered I₂. I₂ guests were modeled with five isolated iodine atom peaks. Fractional iodine atom occupancies are given in parentheses, C) Arrangement of iodine atoms around one cycle. Iodine atoms shown with van der Waals radii, D) Zigzag pattern of disordered I₂ in cycle tubes.

X-ray intensity data from a brownish-red needle were collected at 100(2) K using a Bruker D8 QUEST diffractometer equipped with a PHOTON-100 CMOS area detector and an Incoatec microfocus source (Mo K α radiation, $\lambda = 0.71073$ Å). The raw area detector data frames were reduced, scaled and corrected for absorption effects using the Bruker APEX3, SAINT+ and SADABS programs.^{1,2} The structure was solved with SHELXT.³ Subsequent difference Fourier calculations

and full-matrix least-squares refinement against F^2 were performed with SHELXL-2018³ using OLEX2.⁴

The compound crystallizes in the monoclinic system. The pattern of systematic absences in the intensity data was consistent with the space group $P2_1/c$, which was confirmed by structure solution. The asymmetric unit consists of half of one cyclic $C_{42}H_{36}Br_2N_6O_2$ molecule located on a crystallographic inversion center, and a zigzag pattern of severely disordered electron density in the tubular interior of the stacked cycles. A satisfactory disorder model could not be achieved for the disordered species despite considerable modeling effort. The observed electron density is most consistent with iodine, presumably from diiodine molecules. Disorder models involving other guest species, such as the crystallization solvents DMSO or dimethoxyethane, were not successful. Trial refinements of the intra-tube electron density as carbon or oxygen atoms gave physically impossible occupation factors, two of which were much greater than 100% C or O. This observation is consistent with the presence of atoms much heavier than oxygen in the channels, *i.e.* the soaking reagent iodine. Discrete I_2 molecules could not be resolved within the channels, nor could the peaks be unambiguously fitted to diiodine molecules using distance restraints. It is likely that the I_2 molecules are continuously disordered over multiple sites within the observed sinusoidal chains. For the disorder model, iodine peaks were added to the refinement until the largest residual peak was less than $1 e^-/\text{\AA}^3$. Individual iodine site occupancies refined to: I1, 0.153(3); I2, 0.080(1); I3, 0.045(4); I4, 0.038(3); I5 = 0.026(4). These were refined isotropically, as anisotropic refinement led to extremely elongated ellipsoids. This is also consistent with a smeared-out, non-discrete distribution of iodine within the channels. The typical I-I distance in uncoordinated I_2 is 2.76(4) Å, from a search of the Cambridge Structural Database.⁵ The interatomic distances (Å) between each iodine peak closest to 2.76 Å are I1, 2.62; I2, 2.88; I3, 2.98; I4, 2.79; I5, 2.88. Attempts to restrain pairs of I atoms close to the target distance resulted in significantly poorer *R*-factors and difference map extrema, and also required extremely strict restraints to bring the I atoms close to a 2.76 Å separation. The isolated iodine model described above was used instead of the Squeeze technique in order to provide an estimate of the I_2 content in the tubular volumes. The Squeeze program was also used to estimate the electron count. A guest-accessible volume of 194 Å³ containing 81 electrons per unit cell was calculated. This

corresponds to 0.76 I₂ per unit cell, or 0.38 I₂ per individual cycle molecule. This is close to the 0.34 I₂ per cycle derived from the disorder model. All non-hydrogen atoms of the cycle were refined with anisotropic displacement parameters. Hydrogen atoms bonded to carbon were located in Fourier difference maps before being placed in geometrically idealized positions and included as riding atoms with $d(\text{C-H}) = 0.95 \text{ \AA}$ and $U_{\text{iso}}(\text{H}) = 1.2U_{\text{eq}}(\text{C})$ for arene hydrogen atoms and $d(\text{C-H}) = 0.99 \text{ \AA}$ and $U_{\text{iso}}(\text{H}) = 1.2U_{\text{eq}}(\text{C})$ for methylene hydrogen atoms. The two urea group hydrogen atoms were located and refined freely. The largest residual electron density peak in the final difference map is $0.78 \text{ e}^-/\text{\AA}^3$ located 1.00 \AA from Br1.

Table S1. Data Collection and refinement for host **1** and its inclusion complexes.

Identification code	1 •C ₆ H ₄ N ₂ S	1 •C ₆ H ₂ Cl ₂ O ₂	1 •I ₂
CCDC	2091812	2091813	2091814
Empirical formula	C ₄₅ H ₃₈ Br ₂ N ₇ O ₂ S _{0.5}	C _{43.88} H _{36.63} Br ₂ Cl _{0.63} N ₆ O _{2.63}	C ₄₂ H ₃₆ Br ₂ I _{0.69} N ₆ O ₂
Formula weight	884.67	871.89	903.51
Temperature/K	100(2)	100(2)	100(2)
Crystal system	monoclinic	monoclinic	monoclinic
Space group	P2 ₁ /c	P2 ₁ /c	P2 ₁ /c
a/Å	15.8195(17)	15.782(5)	15.871(3)
b/Å	4.6302(5)	4.6143(15)	4.6048(10)
c/Å	26.812(3)	26.780(9)	26.839(6)
α/°	90	90	90
β/°	100.182(2)	100.354(5)	100.177(4)
γ/°	90	90	90
Volume/Å ³	1933.0(4)	1918.5(11)	1930.6(7)
Z	2	2	2
ρ _{calc} /cm ³	1.520	1.509	1.554
μ/mm ⁻¹	2.174	2.205	2.692
F(000)	902.0	887.0	905.0

Crystal size/mm ³	0.5 × 0.05 × 0.02	0.38 × 0.03 × 0.02	0.46 × 0.06 × 0.03
Radiation	MoKα (λ = 0.71073)	MoKα (λ = 0.71073)	MoKα (λ = 0.71073)
2θ range for data collection/°	2.616 to 50.422	4.4 to 50.16	2.608 to 52.99
Index ranges	-18 ≤ h ≤ 18, -5 ≤ k ≤ 5, -31 ≤ l ≤ 32	-18 ≤ h ≤ 18, -5 ≤ k ≤ 5, -31 ≤ l ≤ 30	-19 ≤ h ≤ 19, -5 ≤ k ≤ 5, -32 ≤ l ≤ 33
Reflections collected	20014	14472	32724
Independent reflections	3477 [R _{int} = 0.0603, R _{sigma} = 0.0366]	3409 [R _{int} = 0.1100, R _{sigma} = 0.0753]	3965 [R _{int} = 0.0736, R _{sigma} = 0.0379]
Data/restraints/parameters	3477/9/265	3409/7/264	3965/0/269
Goodness-of-fit on F ²	1.071	1.052	1.123
Final R indexes [I ≥ 2σ (I)]	R ₁ = 0.0414, wR ₂ = 0.0818	R ₁ = 0.0514, wR ₂ = 0.0999	R ₁ = 0.0510, wR ₂ = 0.1045
Final R indexes [all data]	R ₁ = 0.0628, wR ₂ = 0.0899	R ₁ = 0.0959, wR ₂ = 0.1137	R ₁ = 0.0727, wR ₂ = 0.1139
Largest diff. peak/hole / e Å ⁻³	0.50/-0.50	0.79/-0.55	0.78/-0.59

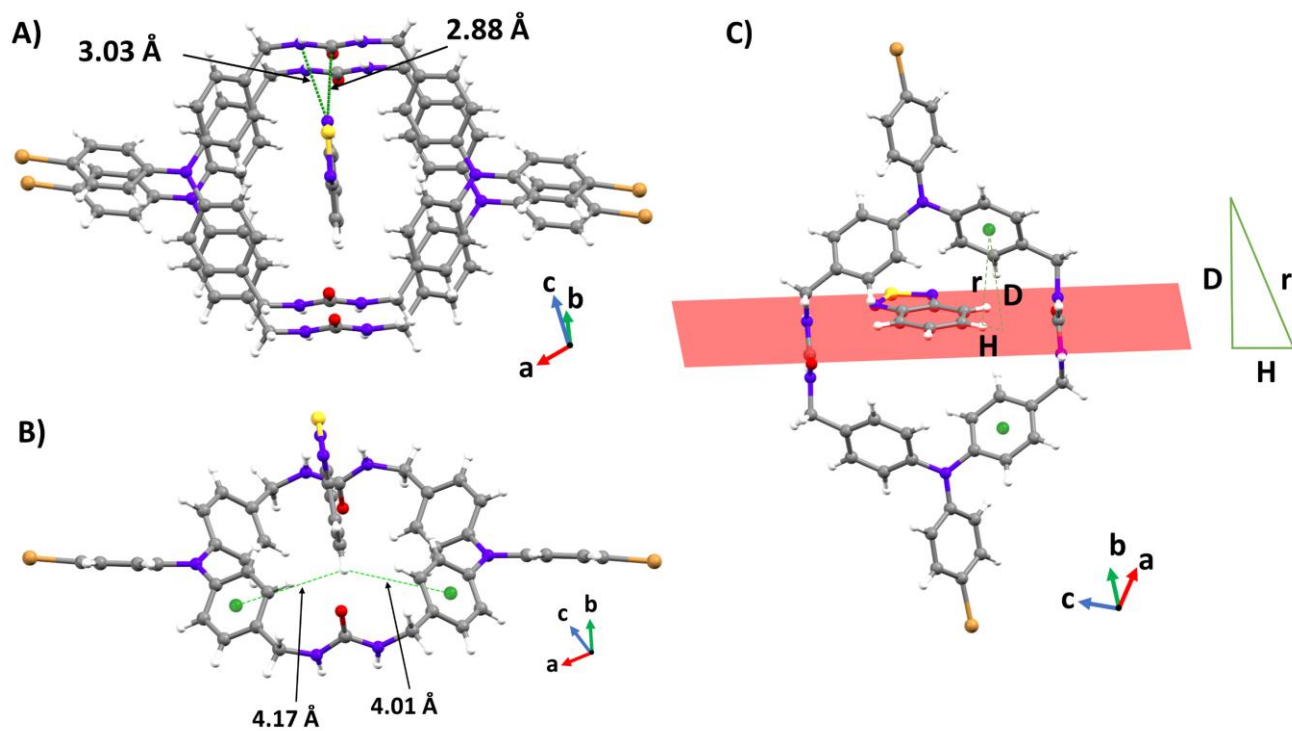


Figure S10. Possible interactions of guest, $C_6H_4N_2S$ with the host **1**. A) N...N interaction between the guest $C_6H_4N_2S$ and host urea, B) Possible C-H... π interaction, C) Orientation of guest with host (Disorder removed for clarity).

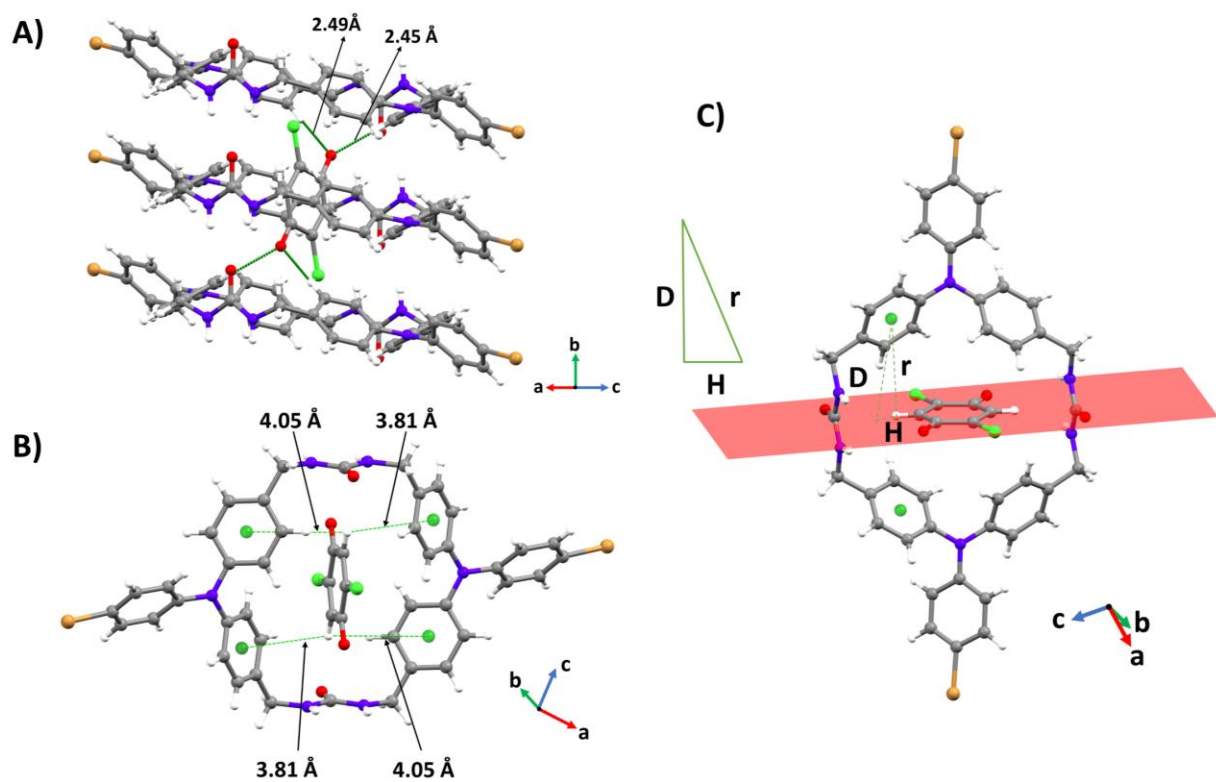


Figure S11. Possible interactions of guest, $C_6H_2Cl_2O_2$ with the host **1**. A) $O...H$ interaction between the guest, $C_6H_2Cl_2O_2$ and host triphenylamine, B) Possible $C-H...π$ interaction, C) Orientation of guest with host (Disorder removed for clarity).

Table S2. Geometric parameters defined for characterizing intramolecular C-H... π stacking interactions (α = plane to plane angle, D= Centroid to plane vertical distance, H= centroid to H offset, r= centroid to H distance).

Compound	α	D	H	r
1•C₆H₄N₂S	65.44	4.11	0.73	4.17
1•C₆H₄N₂S	48.97	3.69	1.54	4.01
1•C₆H₂Cl₂O₂	46.72	3.69	0.90	3.81
1•C₆H₂Cl₂O₂	67.81	4.01	0.61	4.05

Iodine loading in cyclohexane

UV/Vis data was collected on a Shimadzu UV-2600 Spectrophotometer. All data were collected at 25°C. Spectra were recorded from 200-800 nm with 1 nm steps.

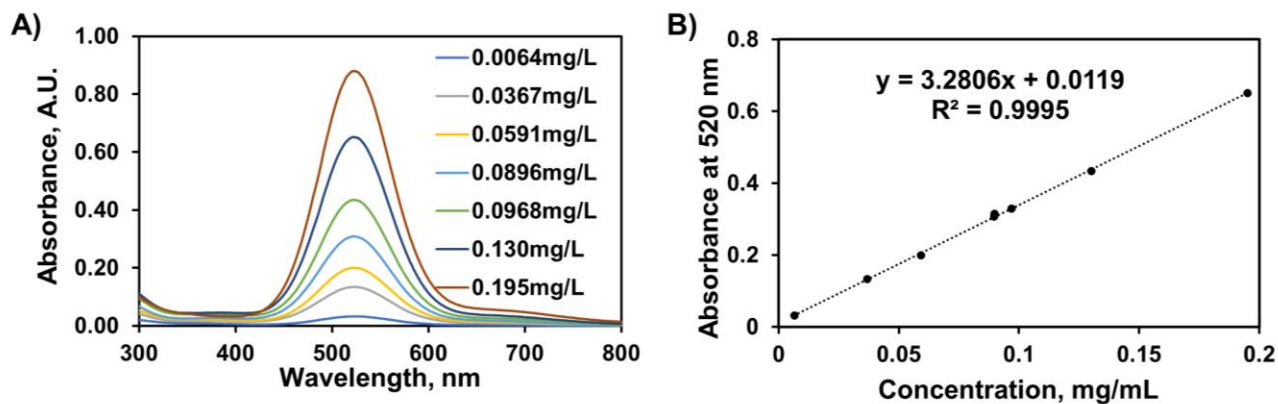


Figure S12. Calibration plot of standard iodine by UV-vis absorption spectra in cyclohexane. A) Absorption spectra of different concentrations of iodine in cyclohexane solution, B) Calibration curve by the fitting of absorbance at 520 nm vs concentration of I_2 .

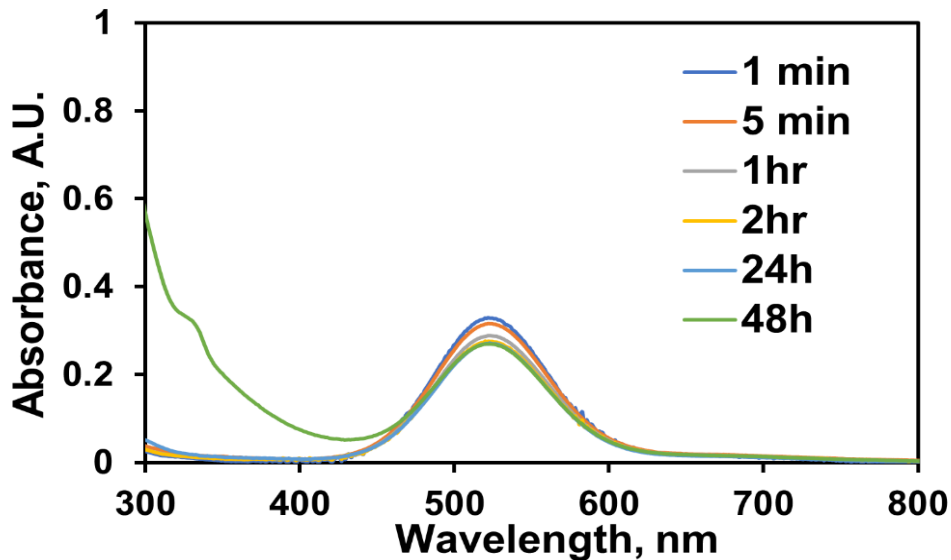


Figure S13. Adsorption of I_2 (Initial = 0.5 mg/mL in cyclohexane) into host **1** (8.5 mg) over time as monitored by UV-vis absorption spectra following loss of I_2 from solution.

Iodine removal in ethanol

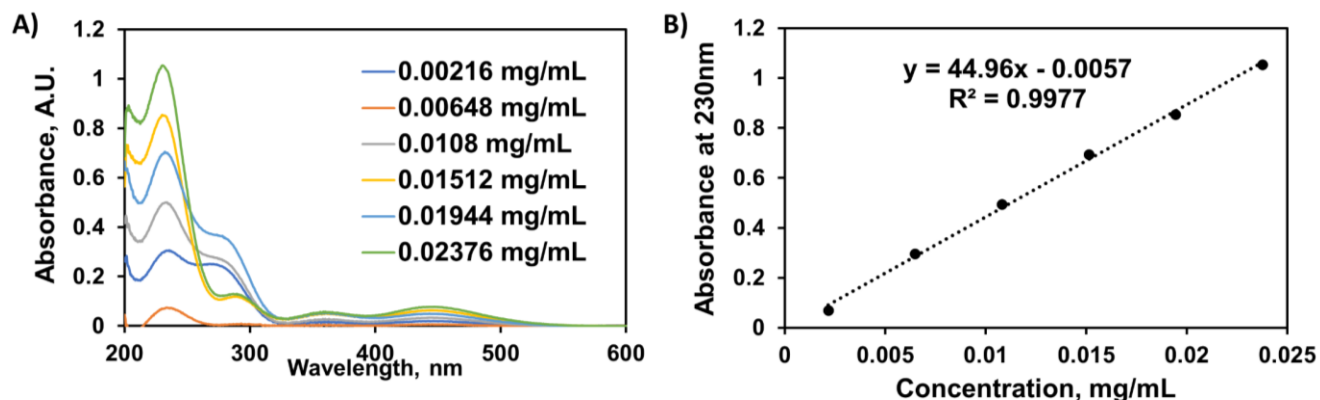


Figure S14. Calibration plot of standard iodine by UV-vis absorption spectra in EtOH. A) Absorption spectra of different concentrations of iodine in EtOH solution, B) Calibration curve by the fitting of absorbance at 230 nm vs concentration of I_2 .

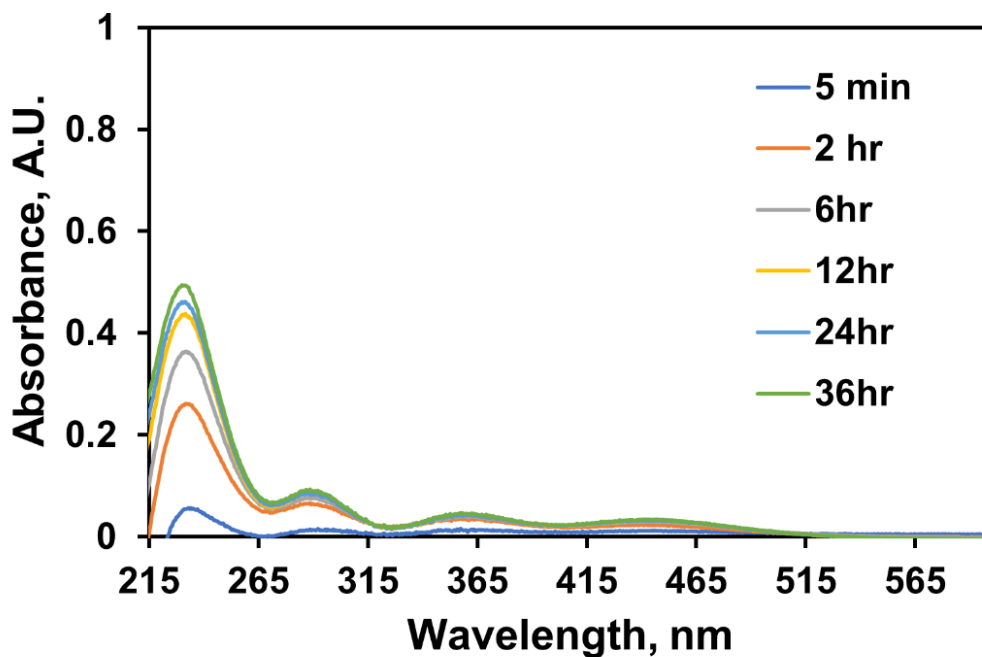


Figure S15. Iodine release over time from $1 \bullet I_2$ in EtOH solution monitored by UV-vis absorption spectra.

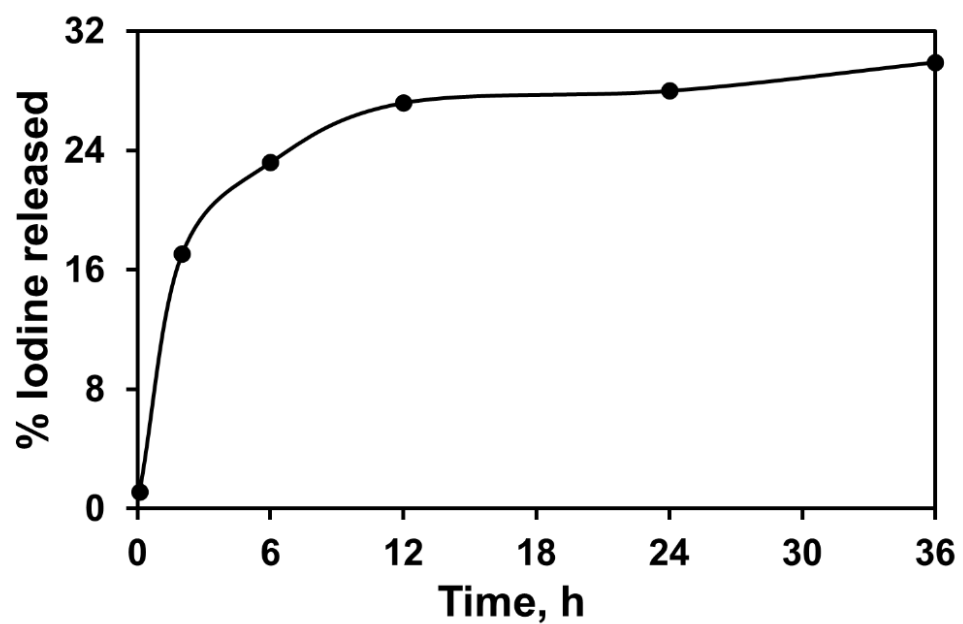


Figure S16. Iodine release over time from $1 \cdot I_2$ (8.5mg) in EtOH solution.

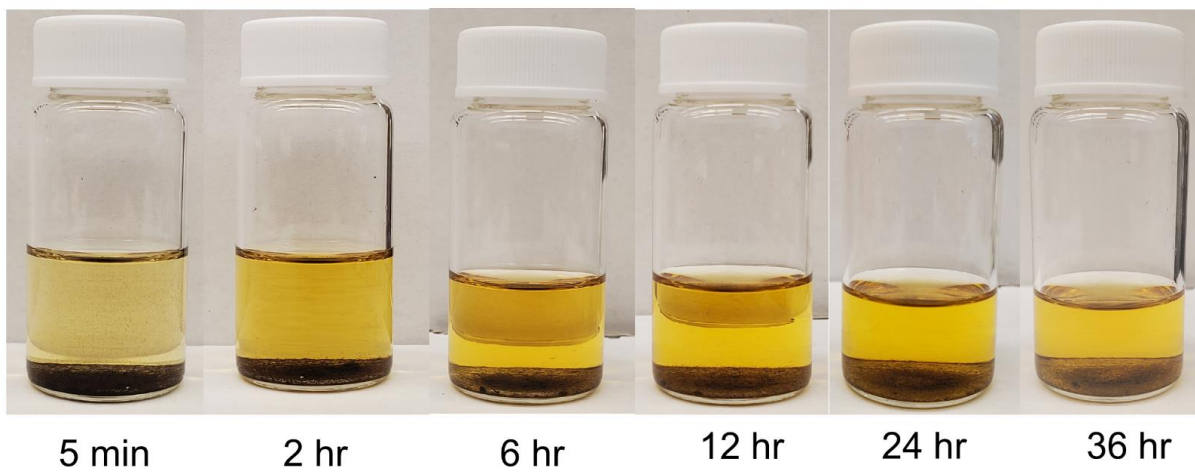


Figure S17. Photograph of I_2 release over time in EtOH.

Solid State Raman Spectrum

Raman spectrum was recorded in Bayspec Nomadic Raman microscope built on an Olympus BX51 reflected optical system. 532nm continuous wave (CW) laser excitation in the confocal mode was used for all the sample. A 50x dark field objective (Olympus LMPLFLN-BD) was used for all the Raman signal collection.

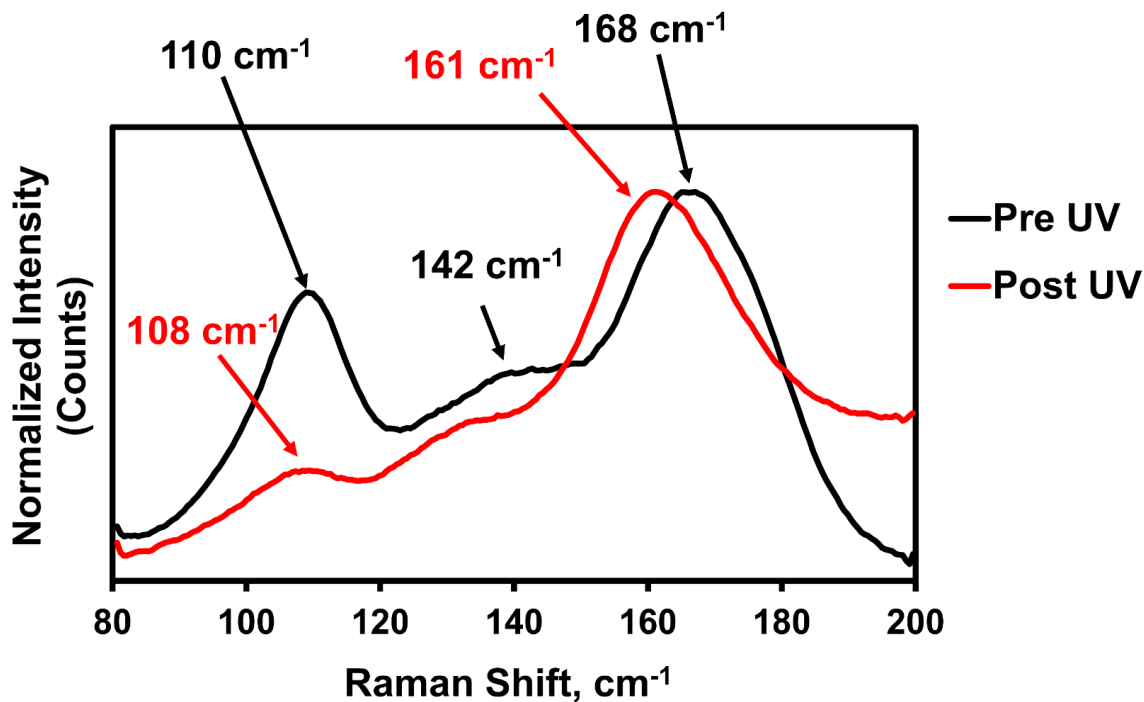


Figure S18. Raman spectra of 1•I₂ complex before and after irradiation with 365nm LEDs.

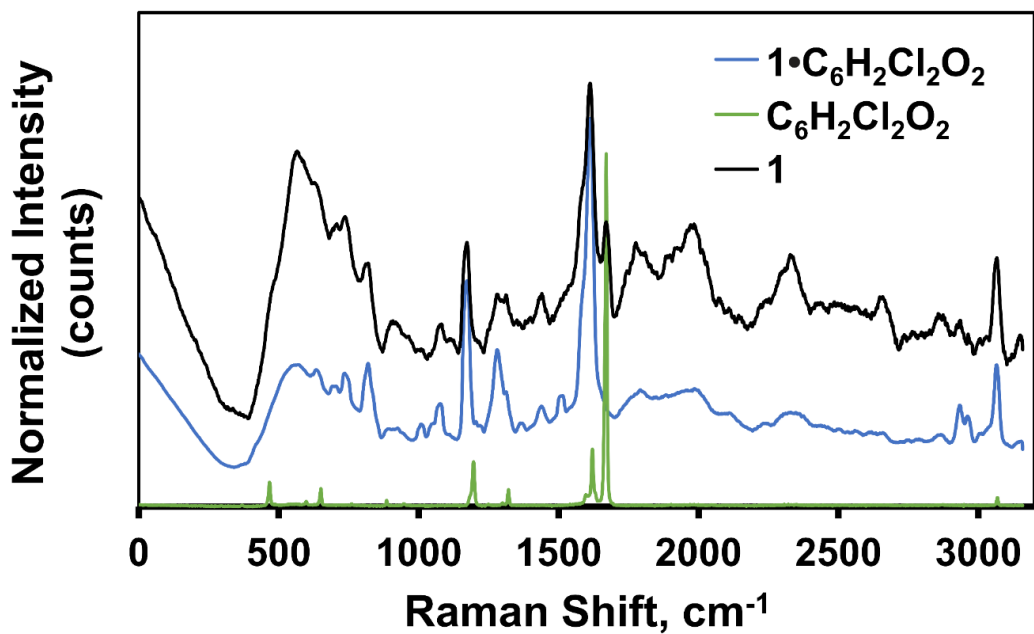


Figure S19. Normalized Raman spectra of Host **1**, $C_6H_2Cl_2O_2$ and $1 \cdot C_6H_2Cl_2O_2$ ($\lambda_{exc} = 532$ nm).

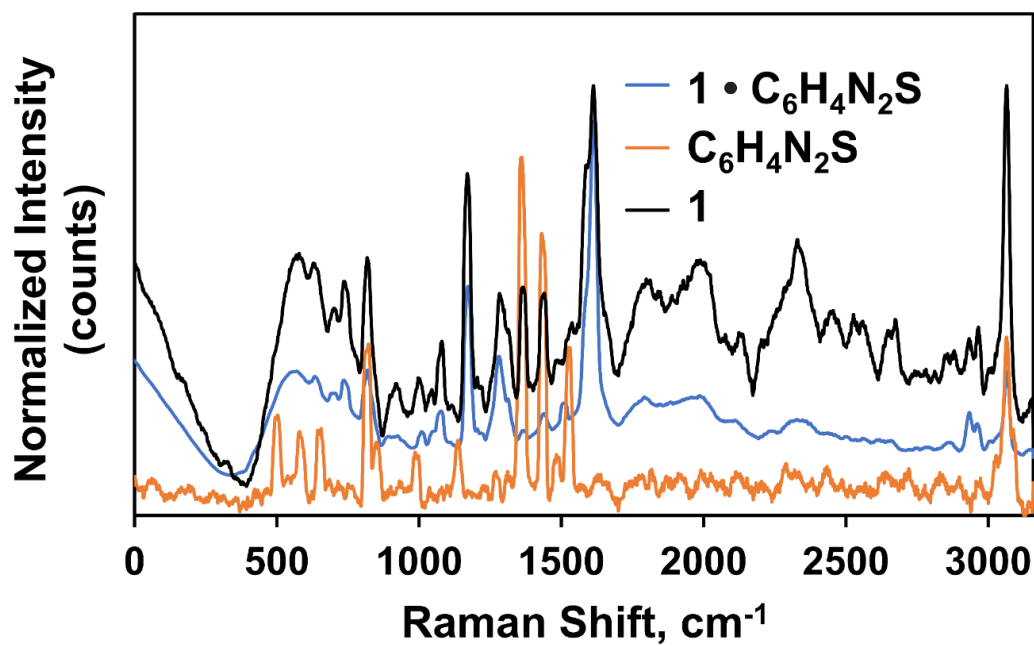


Figure S20. Normalized Raman spectra of Host **1**, $C_6H_4N_2S$ and $1 \cdot C_6H_4N_2S$ ($\lambda_{exc} = 532$ nm).

X-ray Photoelectron spectroscopy (XPS) analysis of $1 \bullet I_2$

XPS analysis was carried out on a Kratos AXIS Ultra DLD XPS system with a monochromatic Al $K\alpha$ source, operated at 15 keV and 150W and at pressures below 10^{-9} torr. The X-rays were incident at an angle of 45° with respect to the surface normal. High resolution core level spectra were measured with a pass energy of 40 eV and analysis of the data was carried out using XPSPEAK41 software. The XPS system was equipped with a hemispherical electron analyzer and a load lock chamber for rapid introduction of samples without breaking vacuum. The XPS experiments were conducted using an electron gun, directed on the sample for charge neutralization. Samples were UV irradiated for 10 hours and used immediately for measurement.

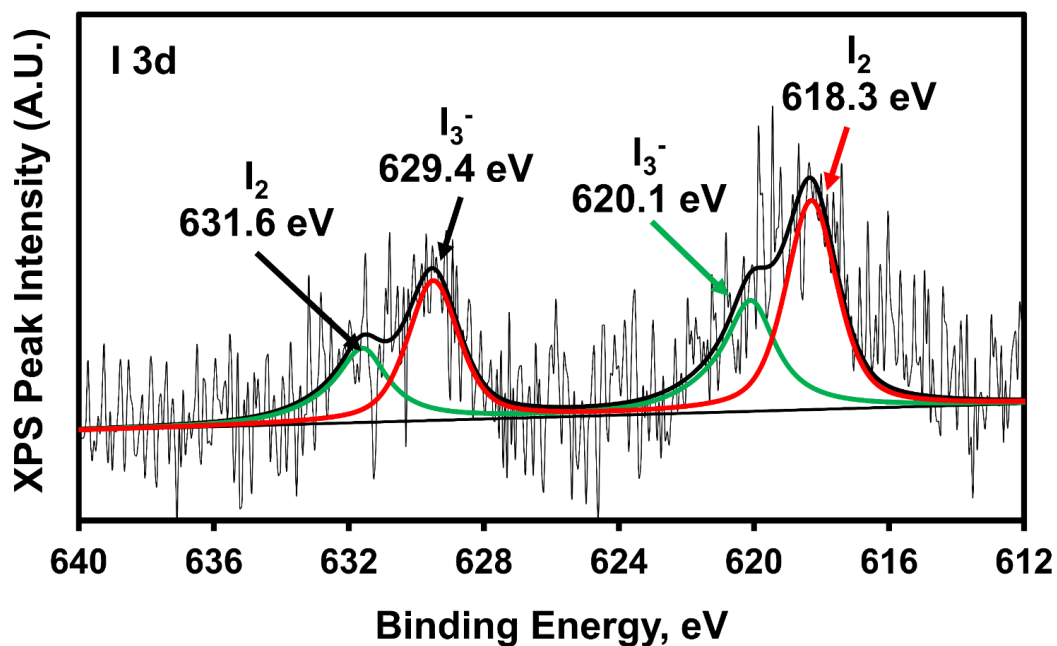


Figure S21. XPS analysis of $1 \bullet I_2$ complex after UV irradiation.

Fourier transform infrared spectra of the complexes

All FT-IR measurements were performed using Perkin Elmer 100 IR spectrometer.

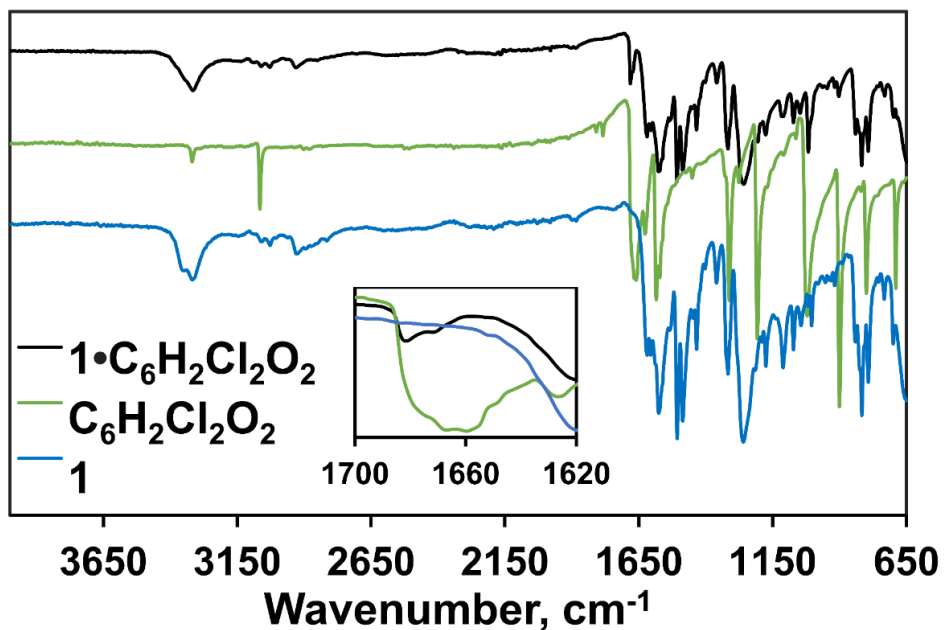


Figure S22. Fourier transform Infrared spectra of Host **1**, C₆H₂Cl₂O₂ and **1**•C₆H₂Cl₂O₂.

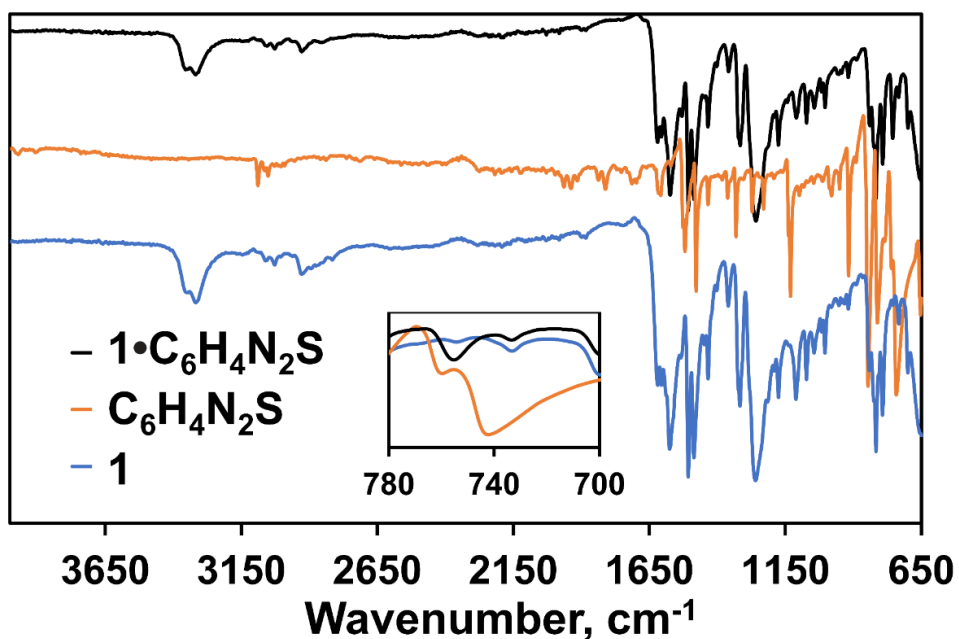


Figure S23. Fourier transform Infrared spectra of Host **1**, C₆H₄N₂S and **1**•C₆H₄N₂S.

Solid State Absorbance measurements

Solid state UV-Vis data was collected on Perkin Elmer Lambda 35 spectrometer with UV vis software. Spectra were recorded from 330-800 nm at 1 nm steps at room temperature.

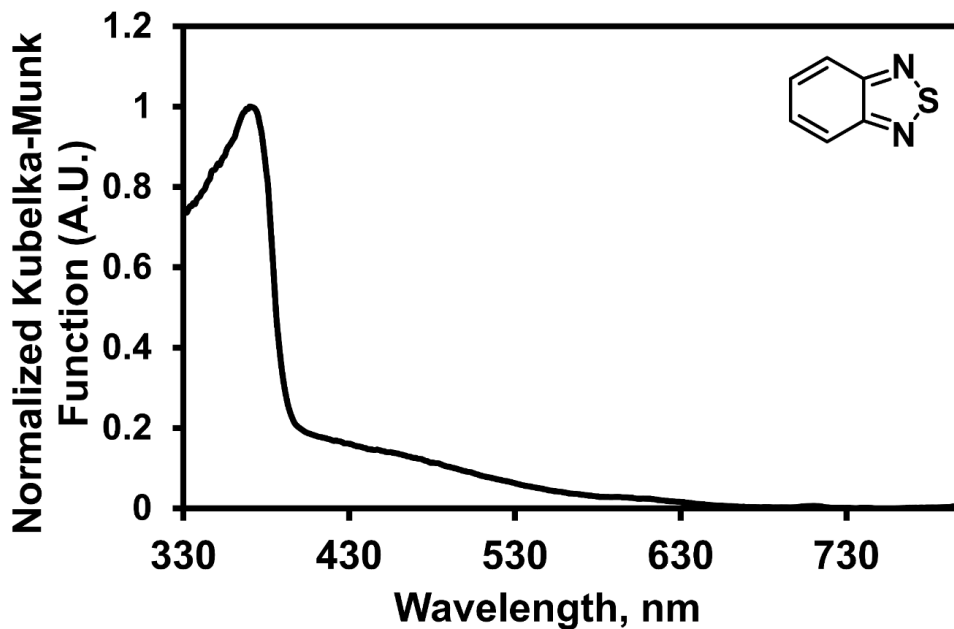


Figure S24. Diffuse reflectance spectra of $C_6H_4N_2S$ in solid state.

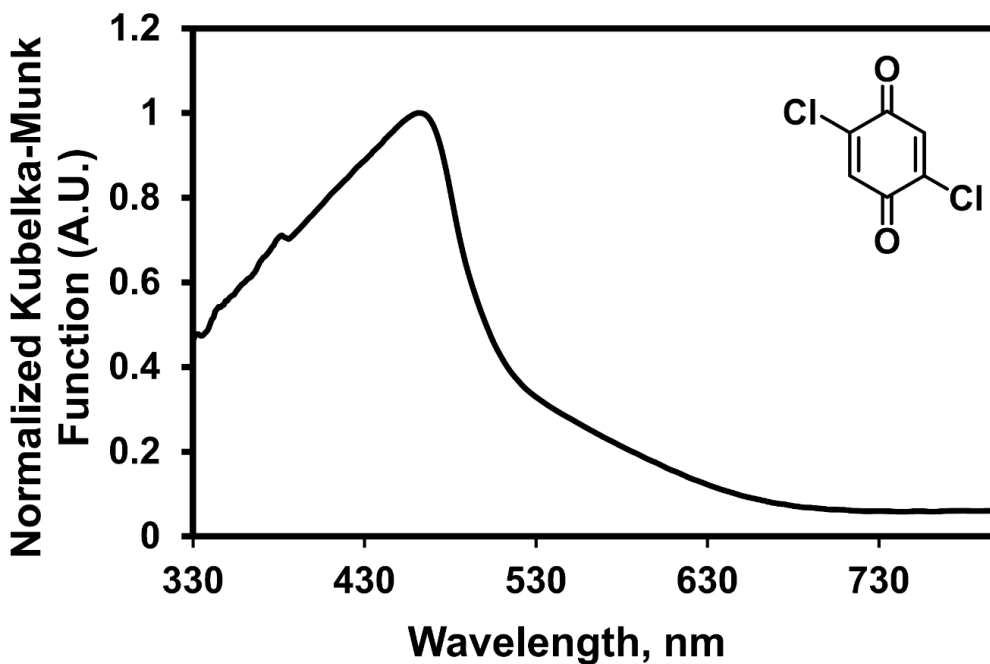


Figure S25. Diffuse reflectance spectra of $C_6H_2Cl_2O_2$ in solid state.

Photoluminescence Measurements

Photoluminescence data was collected on HORIBA Scientific Standard Microscope Spectroscopy Systems connected with iHR320 Spectrometer and Synchrony detector operating on Labspec 6 software. Spectra were recorded using 375nm Laser excitation source power 0.1 mW with 10x UV objective.

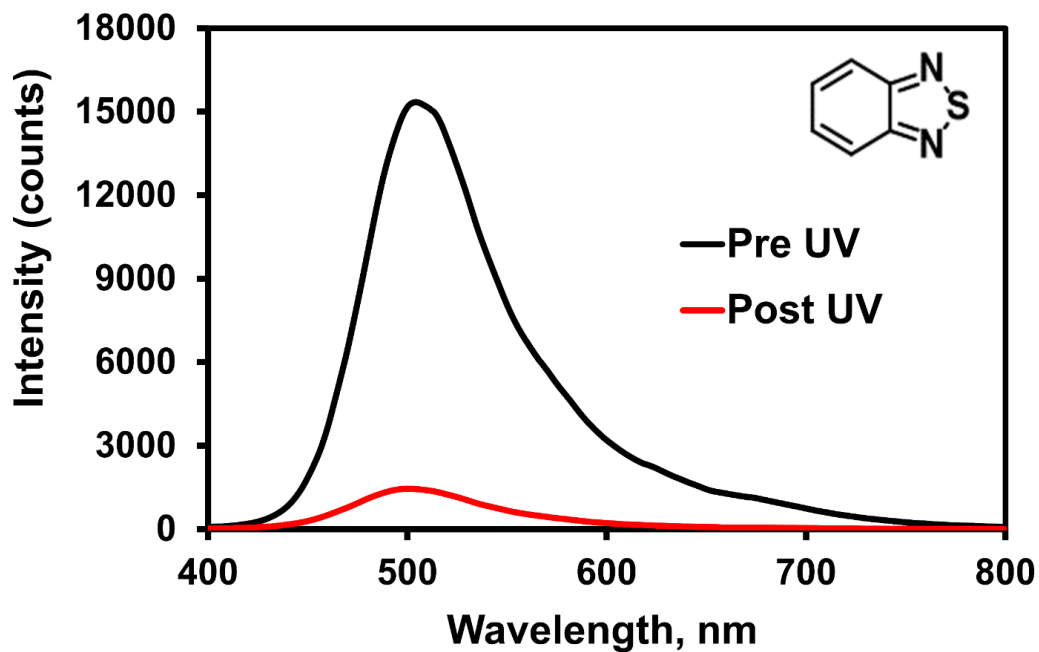


Figure S26. Photoluminescence spectra of 1•C₆H₄N₂S before and after UV irradiation.

(λ_{exc} = 375nm).

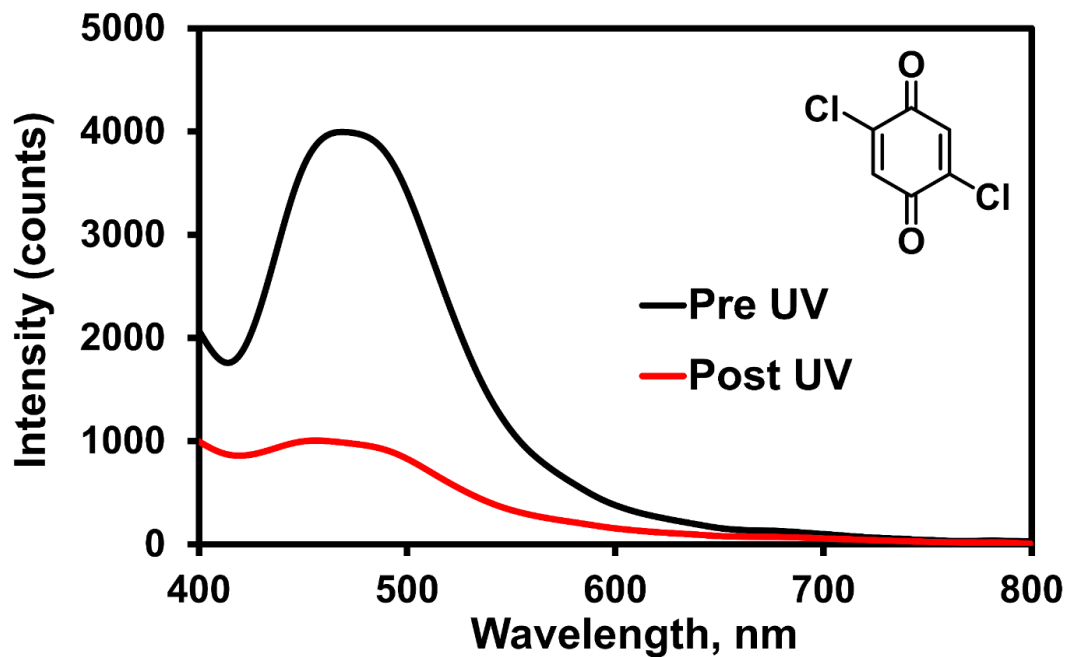


Figure S27. Photoluminescence spectra of **1**•C₆H₂Cl₂O₂ before and after UV irradiation.

($\lambda_{\text{exc}} = 375\text{nm}$).

Cyclic Voltammetry

Cyclic voltammetry Measurements were carried out in dichloromethane using a WaveDriver 20 Bipotentiostat combined with Aftermath software. 0.1M tetrabutylammonium hexafluorophosphate was used as the electrolyte. Measurements were performed in an H cell equipped with a SCE as reference, platinum wire as counter, and glassy carbon as working electrodes. In order to perform CV measurement in solid samples, a slurry was prepared by immersing the crystals in pentane. The slurry was then carefully deposited on the tip of the glassy carbon electrode. The crystals were then dried and used immediately for measurement. Measurements were performed at potential rate of 100mV/s and 50mV/s.

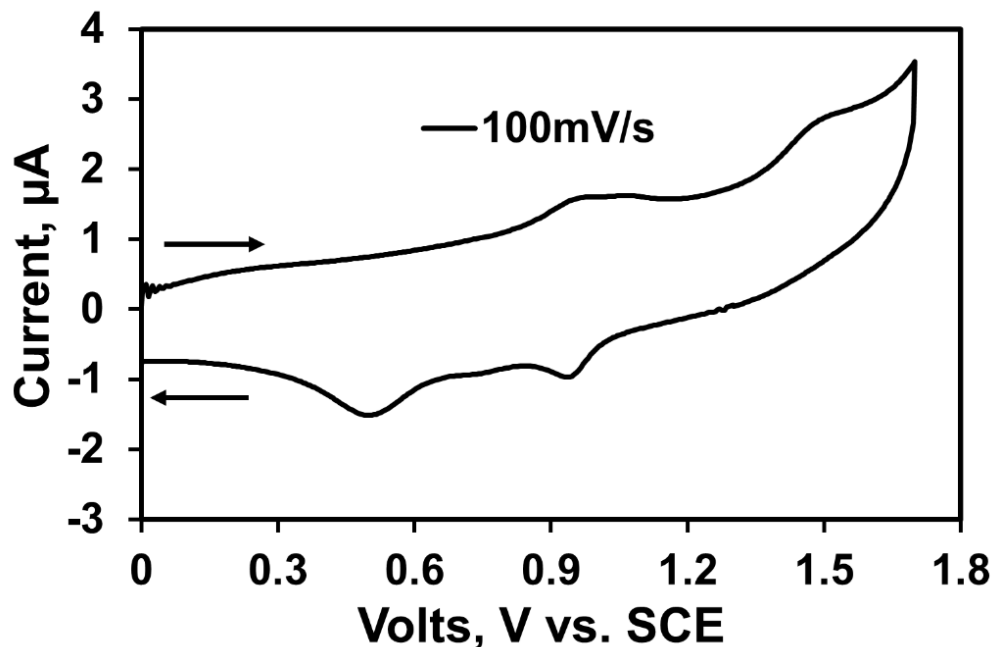


Figure S28. Oxidative cyclic voltammetry of host 1 at 100 mV/s scan rate.

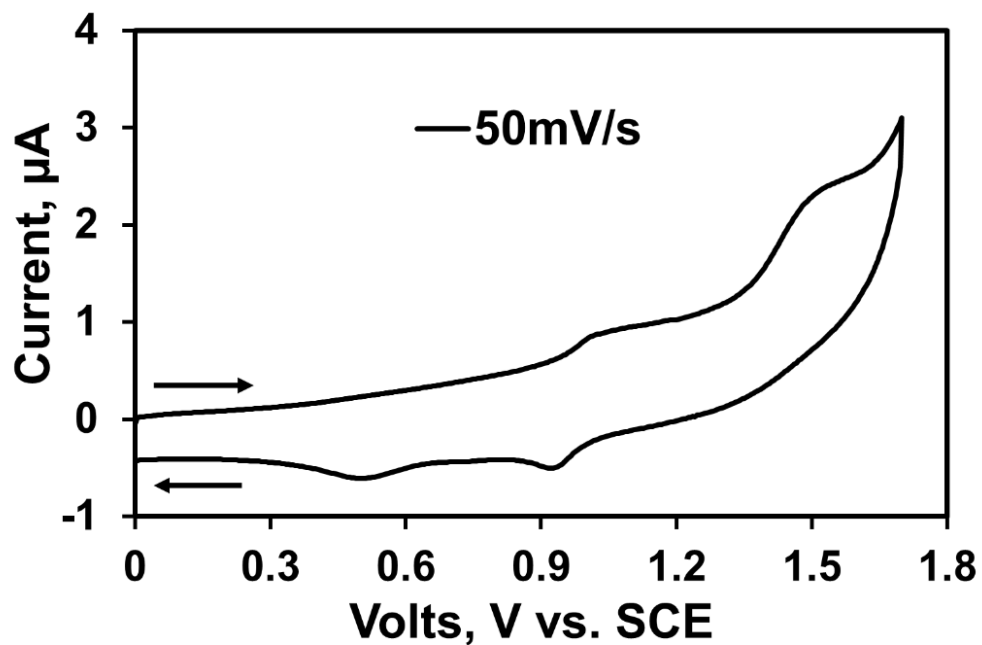


Figure S29. Oxidative cyclic voltammetry of host 1 at 50 mV/s scan rate.

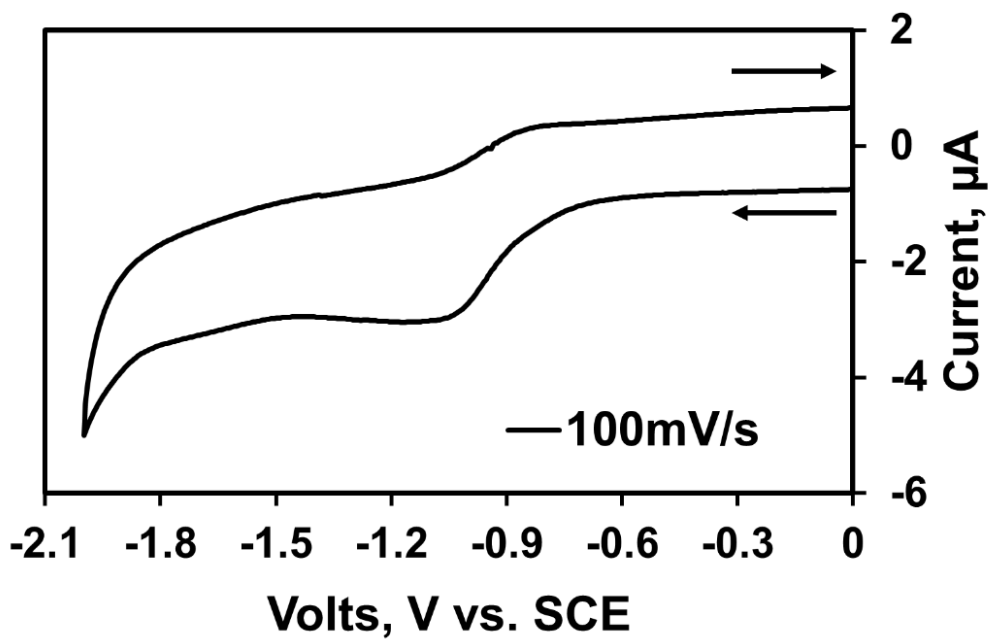


Figure S30. Reductive cyclic voltammetry of host 1 at 100 mV/s scan rate.

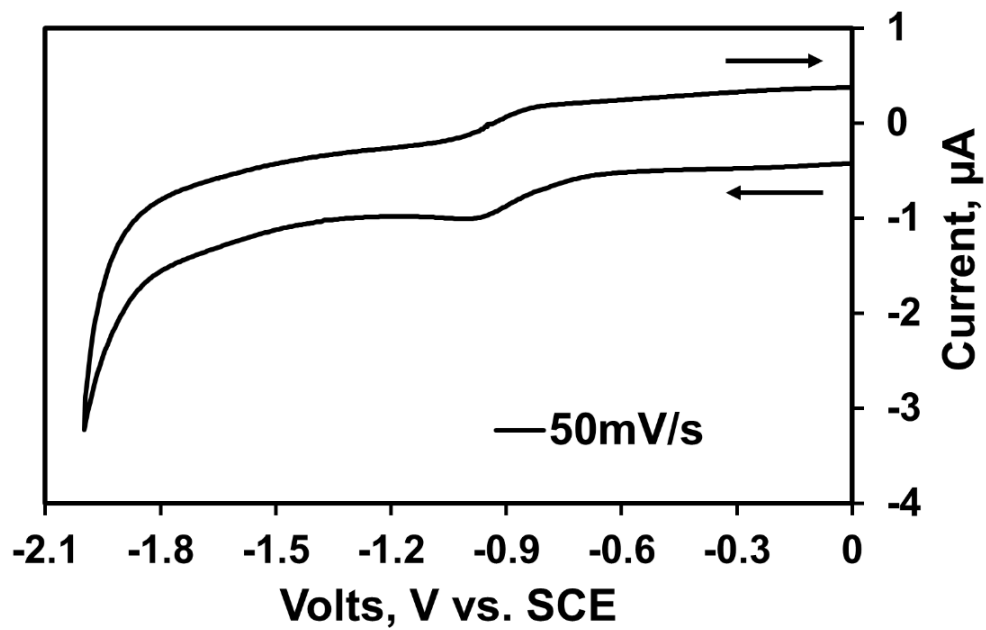


Figure S31. Reductive cyclic voltammetry of host 1 at 50 mV/s scan rate.

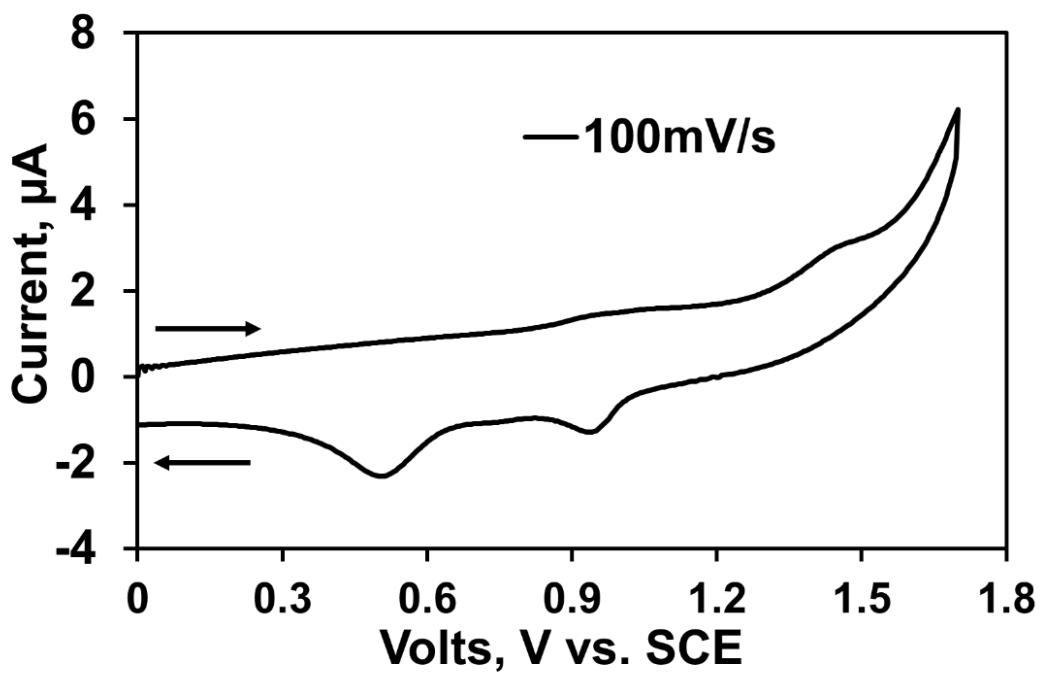


Figure S32. Oxidative cyclic voltammetry of $1 \cdot C_6H_4N_2S$ at 100 mV/s scan rate.

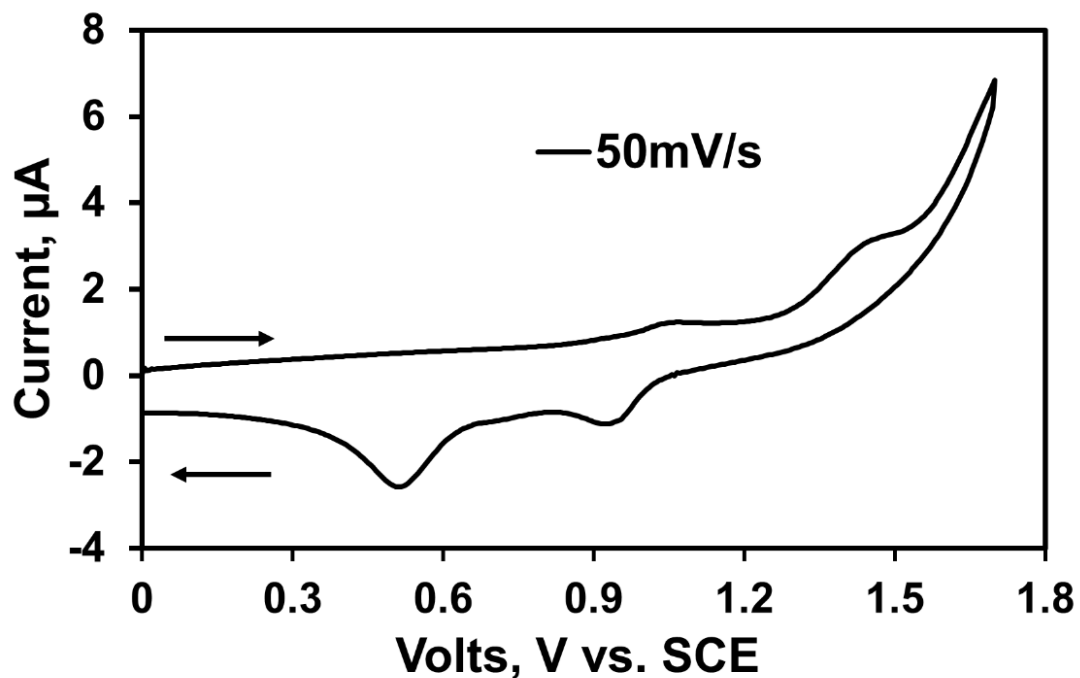


Figure S33. Oxidative cyclic voltammetry of $1\bullet\text{C}_6\text{H}_4\text{N}_2\text{S}$ at 50 mV/s scan rate.

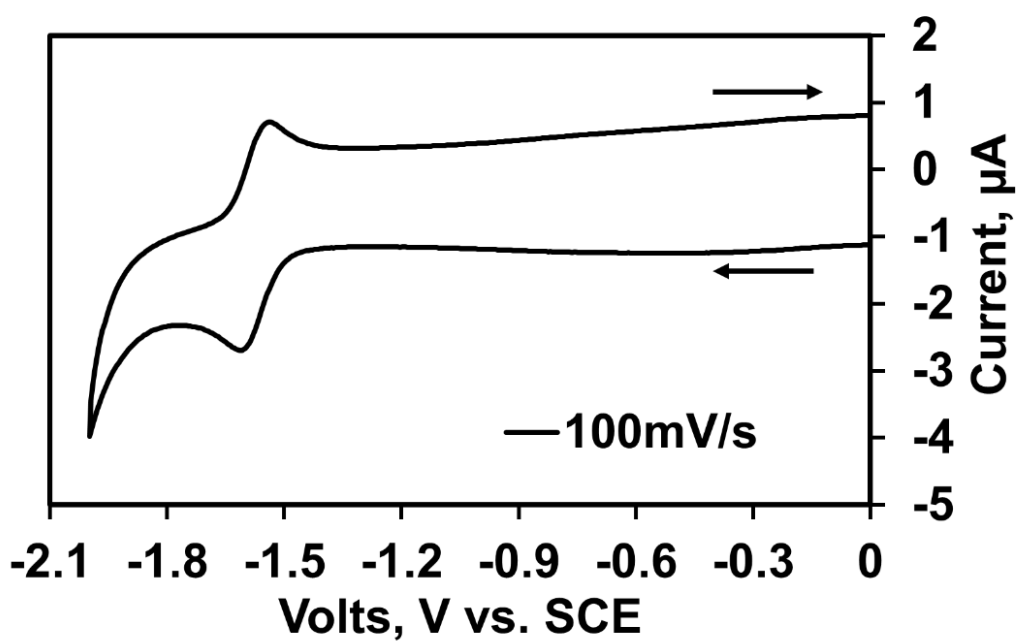


Figure S34. Reductive cyclic voltammetry of $1\bullet\text{C}_6\text{H}_4\text{N}_2\text{S}$ at 100 mV/s scan rate.

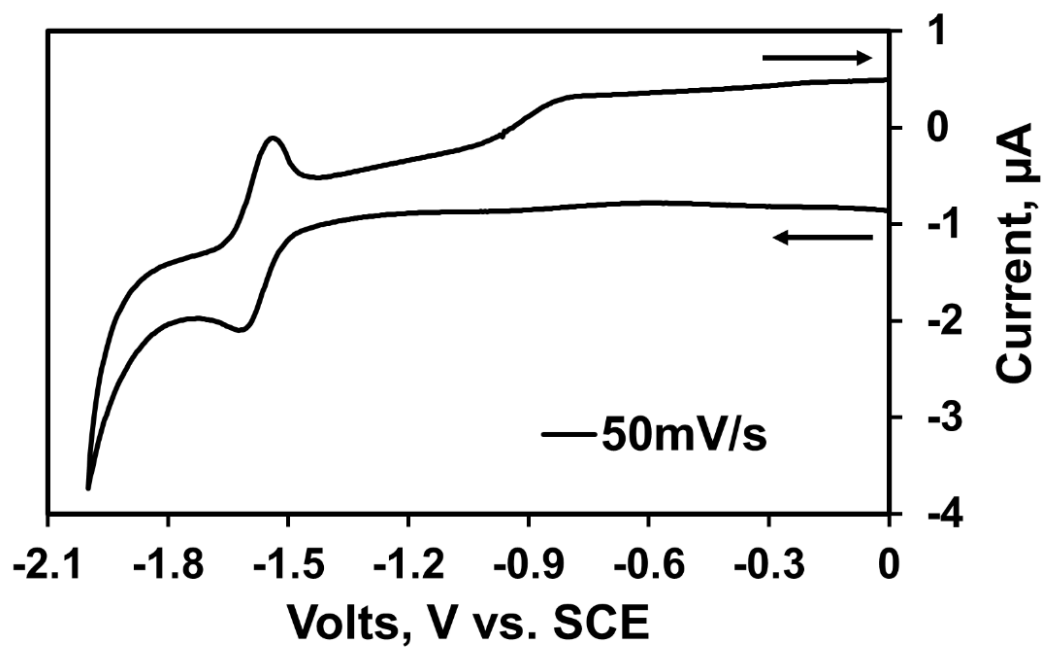


Figure S35. Reductive cyclic voltammetry of $1 \bullet C_6H_4N_2S$ at 50 mV/s scan rate.

Tauc Plot and band gap measurements

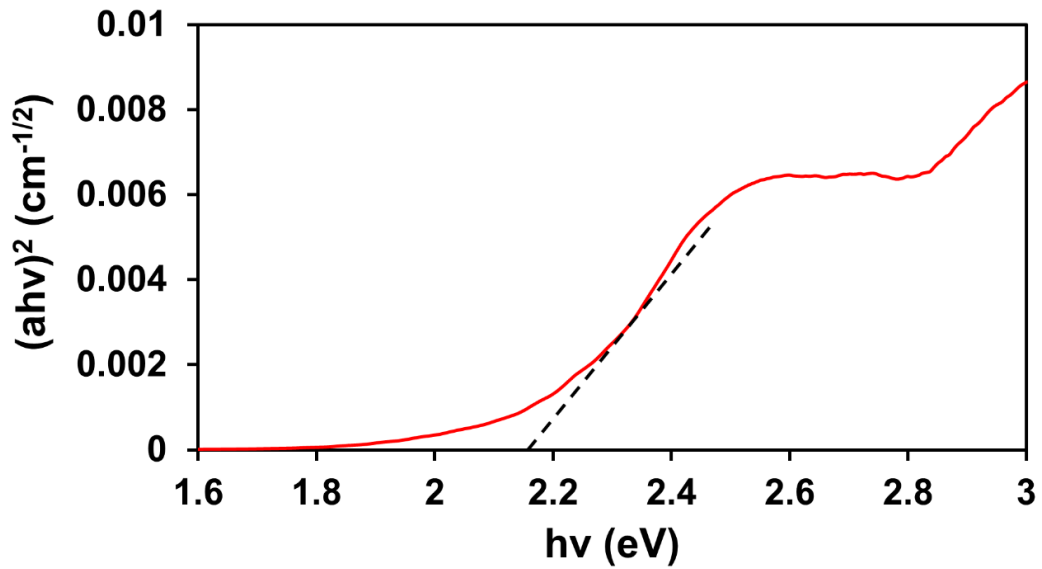


Figure S36. Tauc plot for 1•C₆H₄N₂S.

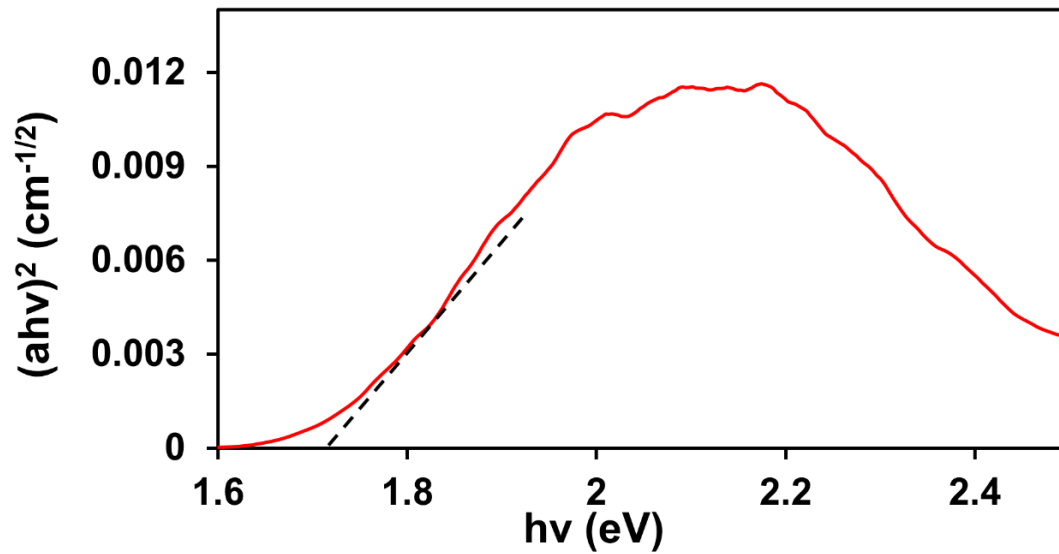


Figure S37. Tauc plot for 1•C₆H₂Cl₂O₂.

Electron Paramagnetic Resonance (EPR) measurements

EPR measurements were carried out on a Bruker EMX plus equipped with a Bruker X-band microwave bridgehead and Xenon software (v 1.1b.66). All EPR spectra were recorded at room temperature. Samples were sealed under Argon and irradiated with 365 nm LEDs. The double integration to obtain peak areas was performed in the Xenon software. Dark decay was done after irradiating the sample up to their maximum radical generation and store them in dark under Argon. EPR spectra were recorded over 3 days. EPR spectra were doubly integrated to obtain the area under the curve and plotted against time after UV irradiation.

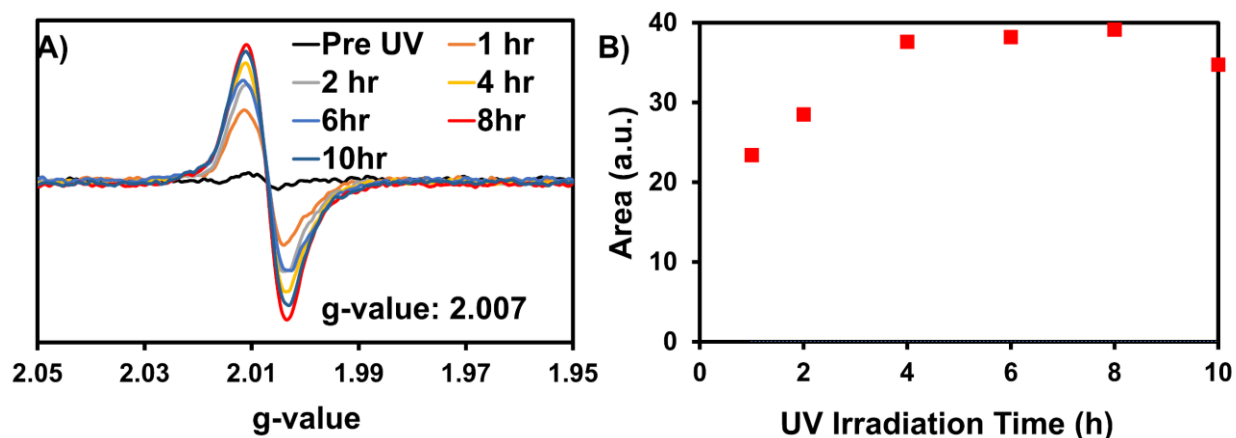


Figure S38. EPR data for 1•C₆H₄N₂S complex (A) EPR spectra over time of UV-irradiation. (B) Double integration over time of UV-irradiation. The maximum radical concentration was estimated as 0.29% for 5.2 mg of macrocycle by averaging the last three data points and comparing to a calibration curve with magic blue.

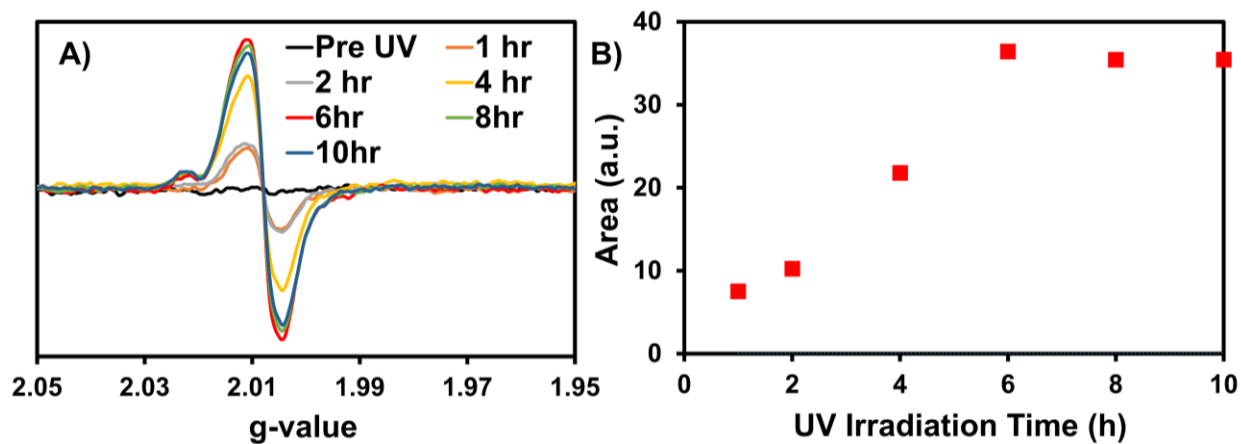


Figure S39. EPR data for $1\bullet\text{C}_6\text{H}_2\text{Cl}_2\text{O}_2$ complex (A) EPR spectra over time of UV-irradiation. (B) Double integration over time of UV-irradiation. A maximum radical concentration of 0.30% was estimated for 5 mg of macrocycle by averaging the last three data points as compared to a calibration curve with magic blue.

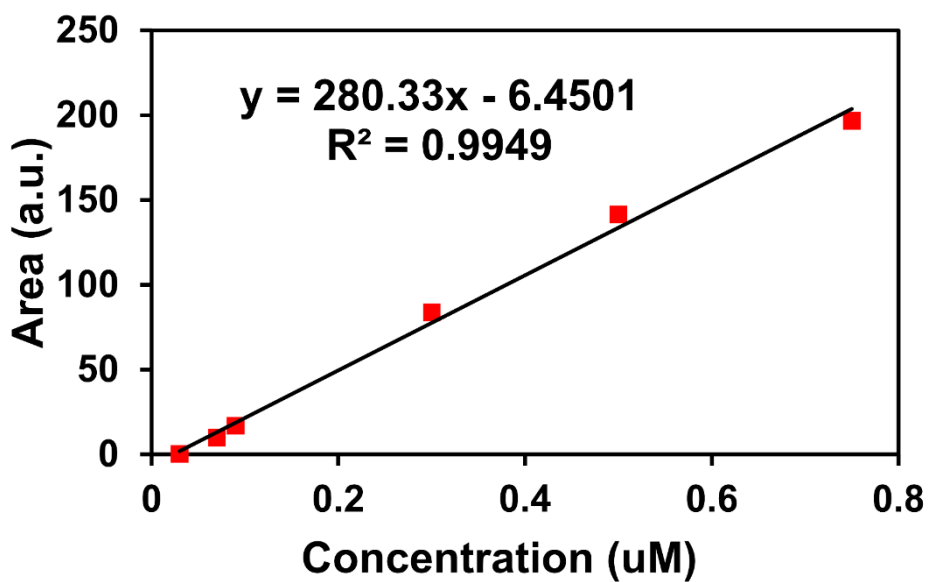


Figure S40. Calibration plot for radical concentration determination for magic blue.

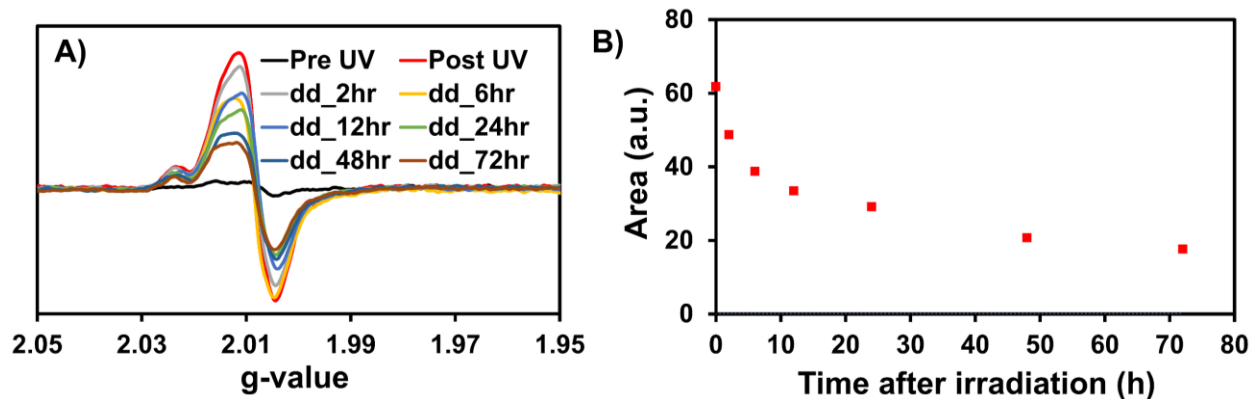


Figure S41. $1\bullet\text{C}_6\text{H}_2\text{Cl}_2\text{O}_2$ complex was initially UV-irradiated to its maximum radical concentration then the light was removed, and the sample monitored by EPR. (A) Dark decay of $1\bullet\text{C}_6\text{H}_2\text{Cl}_2\text{O}_2$ complex after initial UV irradiation, (B) Double integration over time after initial UV irradiation.

NMR Spectra Pre and Post UV

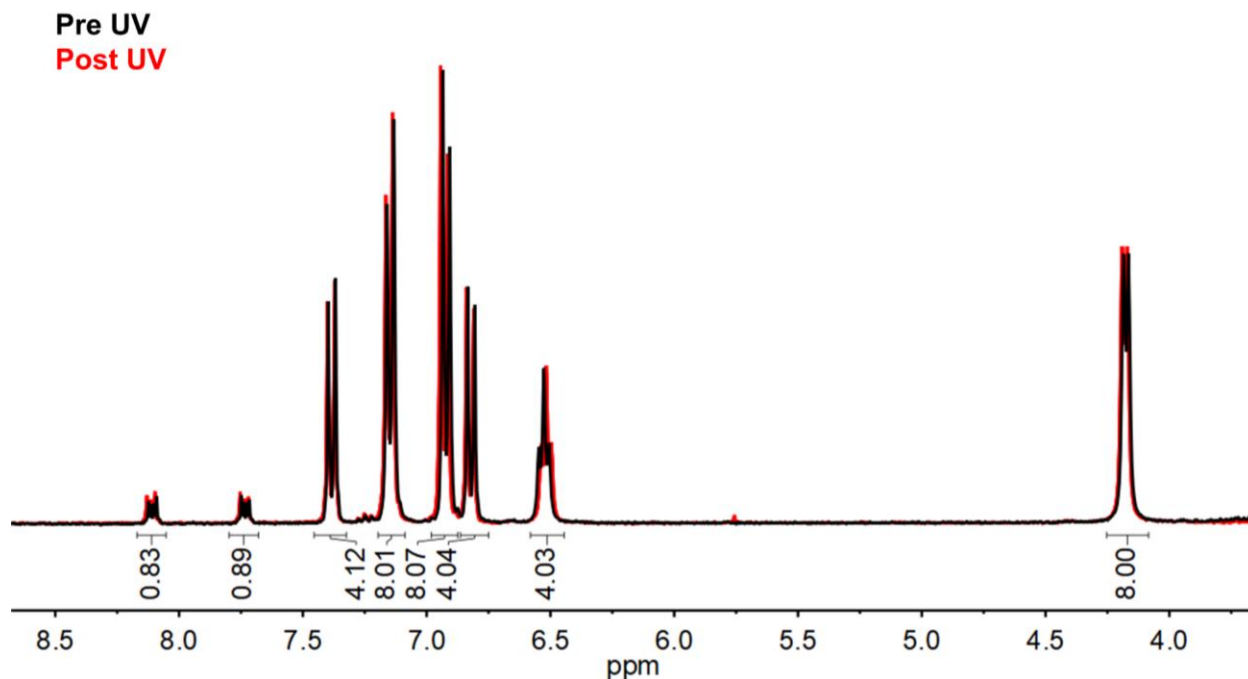


Figure S42. ^1H NMR of $1\bullet\text{C}_6\text{H}_4\text{N}_2\text{S}$ complex after UV irradiation for 6 hours (DMSO- d_6 , 300 MHz). No changes were observed upon UV irradiation.

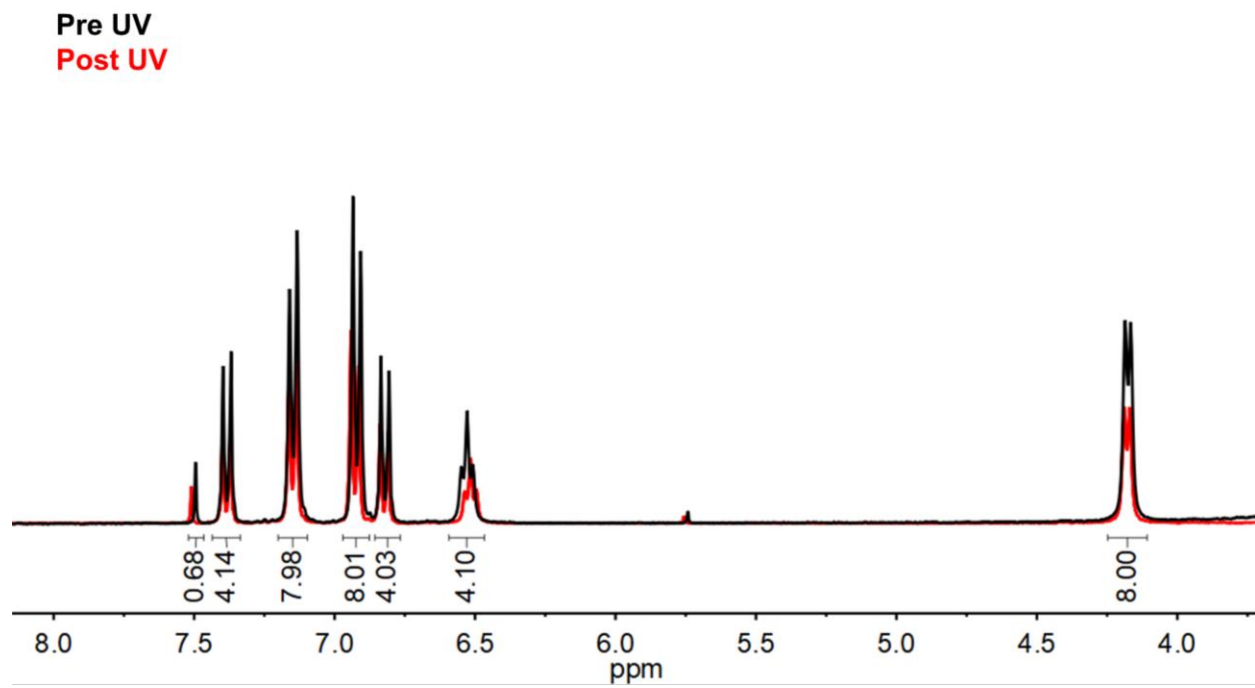


Figure S43. ^1H NMR of $1\bullet\text{C}_6\text{H}_2\text{Cl}_2\text{O}_2$ complex after UV irradiation for 6 hours (DMSO- d_6 , 300 MHz). No changes were observed upon UV irradiation.

IR Spectra Pre and Post UV

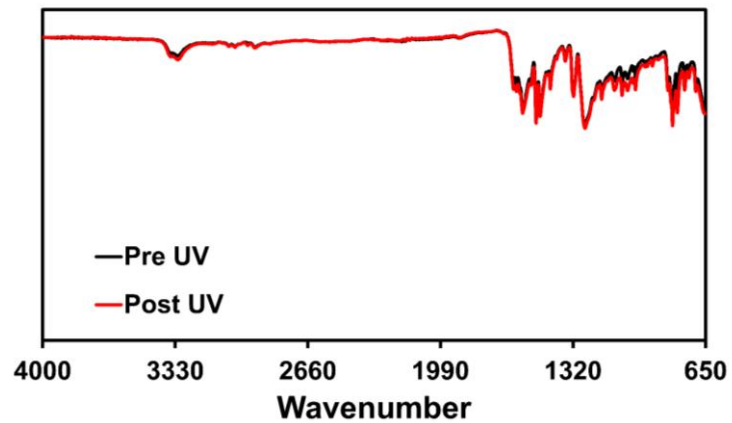


Figure S44. IR spectra of $1 \bullet C_6H_4N_2S$ complex after UV irradiation for 6 hours. No changes were observed upon UV irradiation.

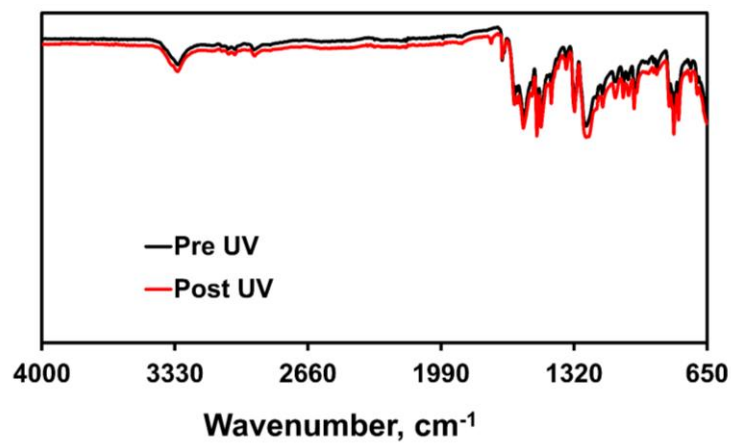


Figure S45. IR spectra of $1 \bullet C_6H_2Cl_2O_2$ complex after UV irradiation for 6 hours. No changes were observed upon UV irradiation.

Computational Details.

All calculations were performed using Q-Chem 5.3.⁸ The spectra were generated by Gaussian-broadening of the spectral lines as given by equation 1. The frontier molecular orbitals (HOMO, LUMO) and the natural transition orbitals (HONTO, LUNTO) were visualized using IQmol v2.14.0 with isovalue 0.04.

$$g(x) = \sqrt{\frac{1}{\pi\sigma^2}} \sum_n f_n e^{-\frac{(x-x_n)^2}{\sigma^2}} \dots\dots\dots (\text{EqS1})$$

In Eq. (1) f_n , and x represents oscillator strength, energy variable (in nm), and the position of n^{th} line (in nm) represents by x_n . The width of the Gaussian was controlled by standard deviation parameter σ set to 20 and 40 nm for $\mathbf{1} \cdot \text{C}_6\text{H}_4\text{N}_2\text{S}$ and $\mathbf{1} \cdot \text{C}_6\text{H}_2\text{Cl}_2\text{O}_2$ complexes, respectively.

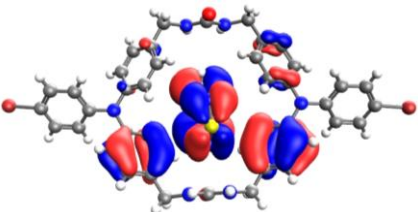
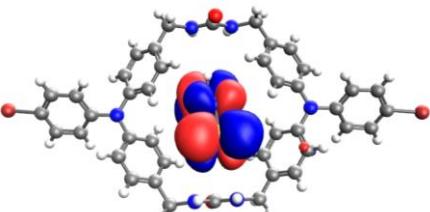
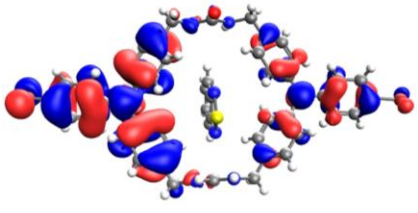
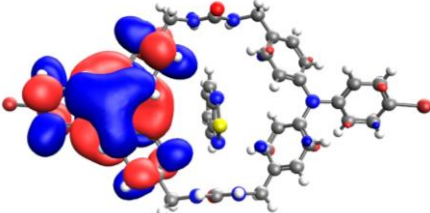
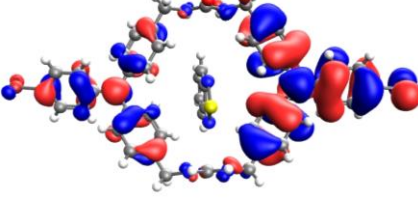
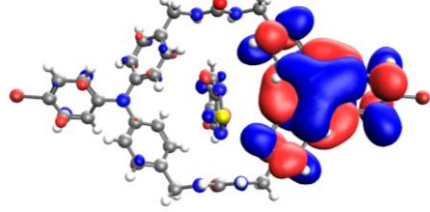
	HOMO-2 -8.098 eV		LUMO -1.744 eV
	HOMO-1 -6.628 eV		LUMO+1 0.146 eV
	HOMO -6.587 eV		LUMO+2 0.179 eV

Figure S46. Calculated Frontier molecular orbitals of $\mathbf{1} \cdot \text{C}_6\text{H}_4\text{N}_2\text{S}$ using CAM-B3LYP/6-31+G** method

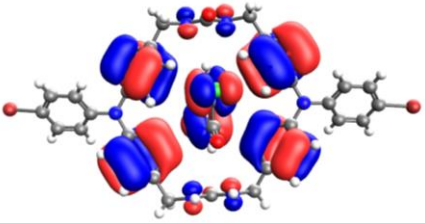
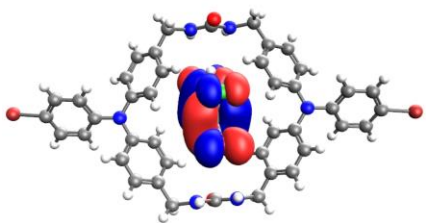
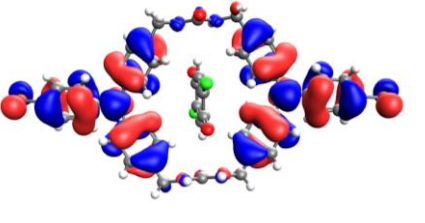
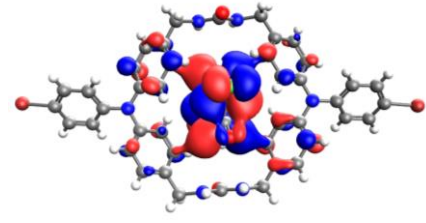
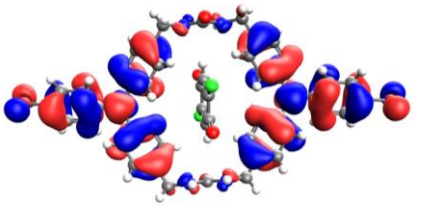
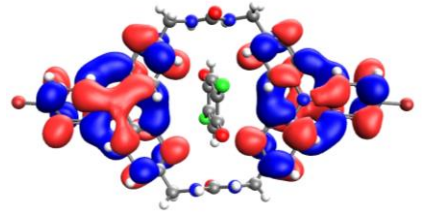
	HOMO-2 -8.435 eV		LUMO -3.347 eV
	HOMO-1 -6.776 eV		LUMO+1 -0.871 eV
	HOMO -6.748 eV		LUMO+2 0.027 eV

Figure S47. Calculated Frontier molecular orbitals of $1 \bullet \text{C}_6\text{H}_2\text{Cl}_2\text{O}_2$ using CAM-B3LYP/6-31+G** method.

Table S3. Excited state transition of $1 \bullet \text{C}_6\text{H}_4\text{N}_2\text{S}$ in gas phase obtained by TD-DFT based on CAM-B3LYP /6-31G**. SC-XRD data of $1 \bullet \text{C}_6\text{H}_4\text{N}_2\text{S}$ was used directly as coordinates. The energies were scaled by multiplying with 0.845 which were used to assign the spectral lines.

State	Energy (nm)	Oscillator Strength
S ₁	794.0347	3.46E-08
S ₂	467.1938	8.11E-07
S ₃	466.0957	9.70E-08
S ₄	462.1907	4.53E-07
S ₅	457.9645	0.002549
S ₆	455.7882	3.74E-08
S ₇	452.6809	9.96E-08
S ₈	451.4554	2.70E-03
S ₉	441.3002	1.46E-06
S ₁₀	440.4657	1.73E-07
S ₁₁	400.4409	2.28E-07
S ₁₂	398.8735	7.31E-07
S ₁₃	396.0209	8.08E-07
S ₁₄	395.2636	3.12E-07
S ₁₅	389.4625	4.48E-07
S ₁₆	381.9808	0.026736
S ₁₇	376.8988	1.85E-07
S ₁₈	355.5572	1.68E-06
S ₁₉	355.041	1.56E-06
S ₂₀	351.7897	0.014321

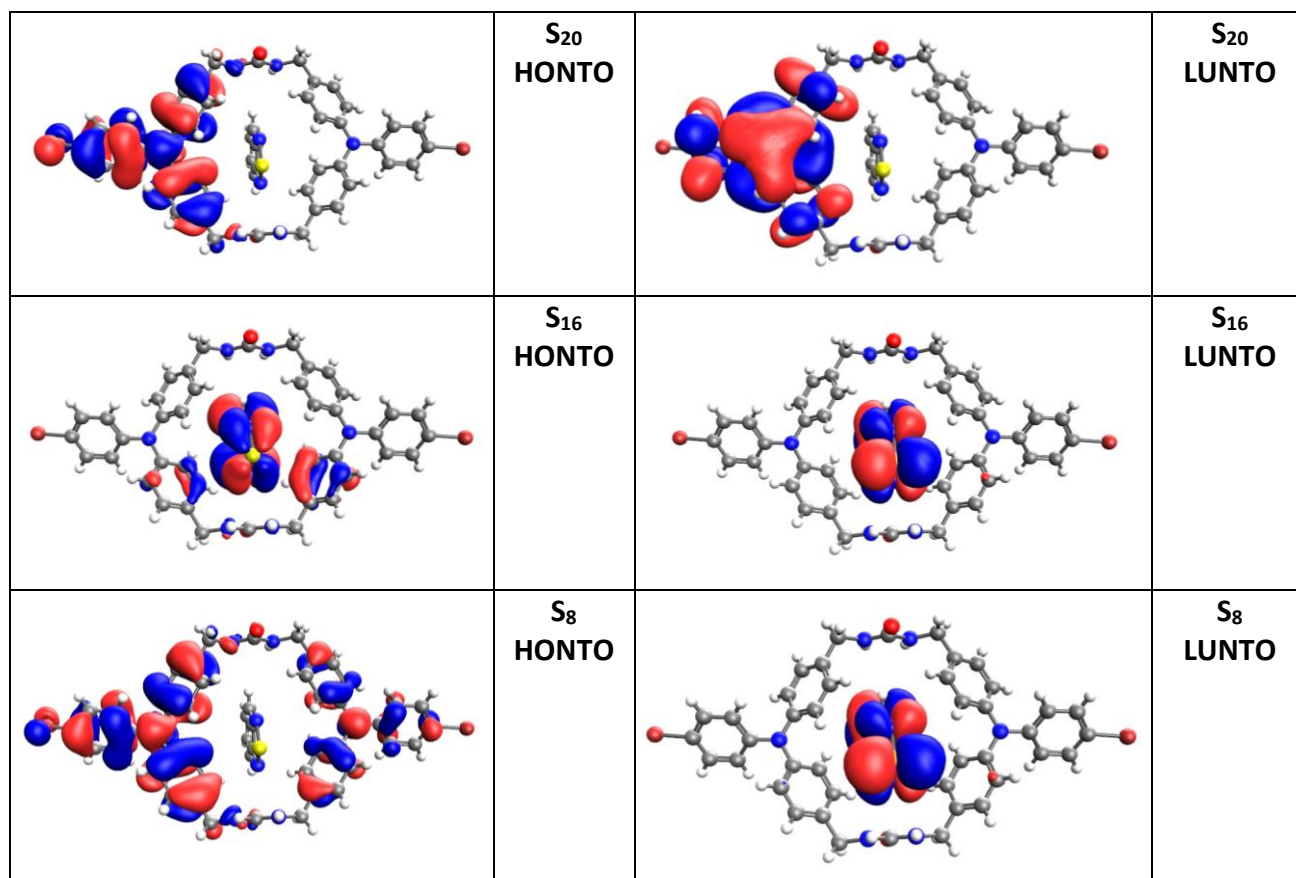


Figure S48. HONTO and LUNTO of corresponding states with high oscillator strength of $1\bullet\text{C}_6\text{H}_4\text{N}_2\text{S}$ in gas phase obtained by TD-DFT based on CAM-B3LYP/6-31+G** method.

Table S4. Excited state transition of **1**•C₆H₄N₂S in gas phase obtained by TD-DFT based on LRC-wPBEH/6-31+G**. SC-XRD data of **1**•C₆H₄N₂S was used directly as coordinates. The energies were scaled by 0.845 which were used to assign the spectral lines.

State	Energy (nm)	Oscillator Strength
S ₁	791.495	1.95E-08
S ₂	475.4141	4.05E-07
S ₃	475.1554	8.12E-08
S ₄	457.7497	2.77E-08
S ₅	454.2758	1.21E-06
S ₆	452.9176	4.75E-07
S ₇	430.66	1.18E-06
S ₈	428.8065	2.68E-03
S ₉	424.4298	1.05E-07
S ₁₀	422.5572	2.39E-03
S ₁₁	406.9876	1.24E-07
S ₁₂	405.9748	2.78E-07
S ₁₃	400.7905	4.87E-08
S ₁₄	400.2718	5.58E-08
S ₁₅	393.9307	2.25E-08
S ₁₆	387.1806	5.81E-08
S ₁₇	380.9999	2.31E-02
S ₁₈	360.5323	3.44E-07
S ₁₉	359.8158	5.13E-07
S ₂₀	351.7505	0.013576

Table S5. Excited state transition of **1**•C₆H₂Cl₂O₂ in gas phase obtained by TD-DFT based CAM-B3LYP/6-31G**. SC-XRD data of **1**• C₆H₂Cl₂O₂ was used directly as coordinates. The energies were scaled by 1.0754 which were used to assign the spectral lines.

State	Energy (nm)	Oscillator Strength
S ₁	1512.929	1.06E-08
S ₂	1166.663	0
S ₃	681.7116	0
S ₄	678.9349	0
S ₅	668.8549	2.76E-08
S ₆	664.82	0.000141
S ₇	640.119	4.70E-08
S ₈	625.2619	0
S ₉	519.2944	0
S ₁₀	508.1533	1.19E-05
S ₁₁	494.7119	0
S ₁₂	424.1534	0
S ₁₃	424.1534	7.75E-08
S ₁₄	410.6603	3.90E-06
S ₁₅	408.5466	0
S ₁₆	404.6415	0.024654
S ₁₇	394.9344	9.43E-07
S ₁₈	388.729	0
S ₁₉	383.8172	1.90E-07
S ₂₀	380.9662	0.031233

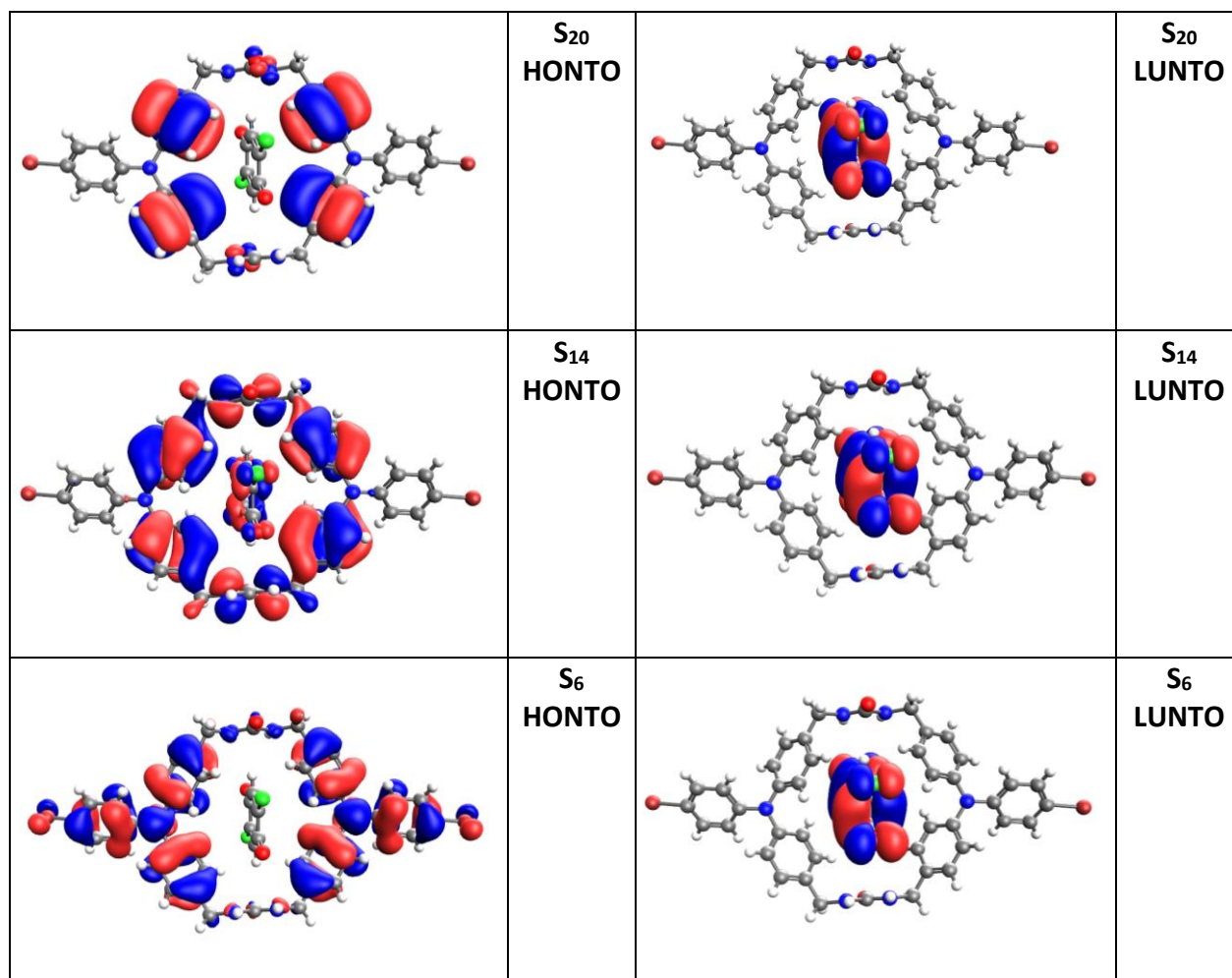


Figure S49. HONTO and LUNTO of corresponding states with high oscillator strength of **1•C₆H₂Cl₂O₂** in gas phase obtained by TD-DFT based on CAM-B3LYP/6-31+G** method.

Table S6. Excited state transition of **1**•C₆H₂Cl₂O₂ in gas phase obtained by TD-DFT based on LRC-wPBEH/6-31G**. SC-XRD data of **1**• C₆H₂Cl₂O₂ was used directly as coordinates. The energies were scaled by multiplying with 1.0762 which were used to assign the spectral lines.

State	Energy (nm)	Oscillator Strength
S ₁	1512.929	1.06E-08
S ₂	1166.663	0
S ₃	681.7116	0
S ₄	678.9349	0
S ₅	668.8549	2.76E-08
S ₆	664.82	0.000141
S ₇	640.119	4.70E-08
S ₈	625.2619	0
S ₉	519.2944	0
S ₁₀	508.1533	1.19E-05
S ₁₁	494.7119	0
S ₁₂	424.1534	0
S ₁₃	424.1534	7.75E-08
S ₁₄	410.6603	3.90E-06
S ₁₅	408.5466	0
S ₁₆	404.6415	0.024654
S ₁₇	394.9344	9.43E-07
S ₁₈	388.729	0
S ₁₉	383.8172	1.90E-07
S ₂₀	380.9662	0.031233

Table S7. HOMO-LUMO gap for the host **1** represented by 1,2 and 3 macrocycles at experimental geometry using CAM-B3LYP/6-31+G** method.

Method	Units	HOMO	LUMO	HOMO-LUMO gap
CAM-B3LYP/6-31+G**	1	-6.37	0.70	7.07
CAM-B3LYP/6-31+G**	2	-6.28	0.49	6.77
CAM-B3LYP/6-31+G**	3	-6.28	0.41	6.69

Table S8. HOMO-LUMO gap for the host **1** represented by 1,2 and 3 macrocycles after optimizing the H-atoms of the neutral species at PM3 level.

Method	Units	HOMO	LUMO	HOMO-LUMO gap
PM3	1	-8.24	-0.43	7.81
PM3	2	-8.20	-0.52	7.68
PM3	3	-8.17	-0.54	7.63
B3LYP/6-31G	1	-5.19	-0.68	4.51
B3LYP/6-31G	2	-5.14	-0.84	4.30
B3LYP/6-31G	3	-5.11	-0.89	4.21

Table S9. Excited state transition of **1**•C₆H₄N₂S complex obtained from TD-DFT calculations.

Compound	Level of theory	State	Type	ΔE , eV	f^a	RMS electron-hole separation ^b Å	μ , D ^c	$ \langle r_e - r_h \rangle ^d$ Å
1 •C ₆ H ₄ N ₂ S	CAM-	S ₅	CT $\pi\pi^*$	3.2039	0.00258	6.3397	15.1183	3.2367
	B3LYP/	S ₈	CT $\pi\pi^*$	3.2505	0.00269	6.3527	15.8294	3.2275
	6-31+G**	S ₁₆	CT $\pi\pi^*$	3.8419	0.0267	3.5169	7.1397	1.1196
		S ₂₀	$\pi\pi^*$	4.1697	0.0135	4.1185	1.9880	0.3499

^aOscillator strength. ^bRoot-mean-square (RMS) electron-hole separation in angstrom. ^c μ Magnitude of transition dipole moment (TDM) in debye (D). ^dLinear electron (e) / hole (h) distance in angstrom Å. The descriptor computed from transition density matrix and state character.

References.

1. A. J. Sindt, M. D. Smith, S. Berens, S. Vasenkov, C. R. Bowers and L. S. Shimizu, *Chem. Commun.*, 2019, **55**, 5619–5622.
2. APEX3 Version 2018.1-0 and SAINT+ Version 8.38A. Bruker AXS, Inc., Madison, Wisconsin, USA, 2016.
3. SADABS-2016/2: Krause, L., Herbst-Irmer, R., Sheldrick G.M. and Stalke D. *J. Appl. Cryst.*, 2015, **48**, 3-10.
4. (a) SHELXT: Sheldrick, G.M. *Acta Cryst.* 2015, **A71**, 3-8. (b) SHELXL: Sheldrick, G.M. *Acta Cryst.*, 2015, **C71**, 3-8.
5. OLEX2: a complete structure solution, refinement and analysis program. Dolomanov, O. V., Bourhis, L. J., Gildea, R. J., Howard J. A. K. and Puschmann, H. *J. Appl. Cryst.*, 2009, **42**, 339-341.
6. Hathwar, V.R.; Gonnade, R.G.; Munshi, P.; Bhadbhade, M.M.; Guru Row, T.N. *Cryst. Growth Des.*, 2011, **11**, 1855-1862.

7. The Cambridge Structural Database. C. R. Groom, C. R., Bruno, I. J., Lightfoot, M. P. and Ward, S. C. *Acta Cryst.*, 2016, **B72**, 171-179.
8. Y. Shao *et al.*, *Mol. Phys.*, 2015, **113**, 184–215.